CHAPTER 5

LOW DIMENSIONALITY SYSTEMS

6.1 INTRODUCTION

In this Chapter, we introduce **low-dimensional structures**, where the electron motion is confined in one or more spatial directions.

When the motion is confined in one direction, we refer to **heterostructures**.

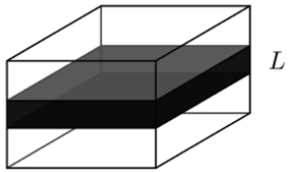

When the motion is confined in two directions, we refer to **nanowires**.

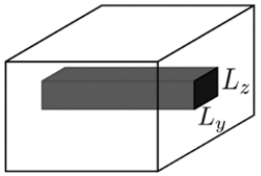

When the motion is confined in all three directions, we refer to **quantum dots**.

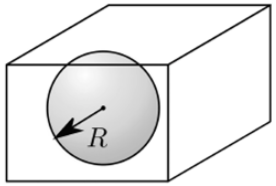

These systems are collectively known as **low-dimensional quantum structures**.

In **Chapter 3**, we already discussed heterostructures, where the electron motion is confined in one direction but remains free in the plane.

Here, we will revisit these two-dimensional systems and introduce one of the most studied 2D structures in recent years, where confinement in one dimension naturally arises from considering a **single atomic layer**, namely **graphene**.

5.2 GRAPHENE

5.2.1 Crystal Structure

The carbon atom has the **electronic configuration** $1s^2$, $2s^2$e $2p^2$, so it has 4 valence electrons.

After the promotion of one electron from the $2s$ orbital to the $2p$ orbital, there are four unpaired electrons available for bonding.

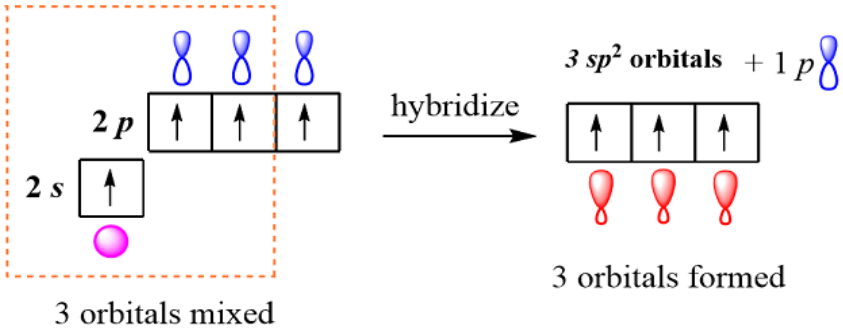

The electron in the shell $2s$ and two electrons in the shell $2p$ form 3 ***sp*² hybrid orbitals**.

These three orbitals lie in the same plane, separated by 120°, forming a trigonal planar geometry and giving rise to **σ-bonds in the plane**.

The remaining $2p$ orbital, which does not participate in hybridization, is oriented **perpendicular to the plane** (the $p_z$orbital).

This orbital overlaps with neighboring p_z orbitals, forming a **π-bond** that extends out of the plane.

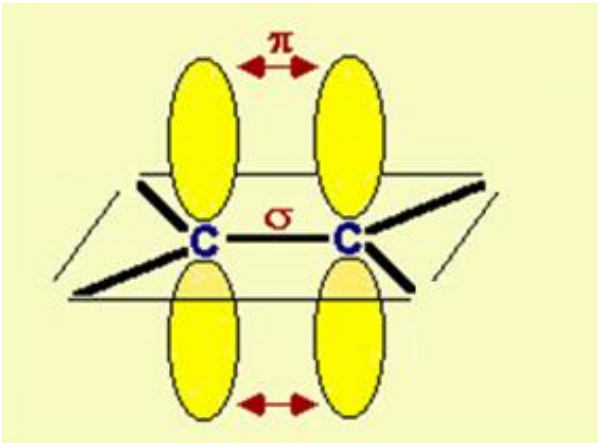

5.2 GRAPHENE

5.2.1 Crystal Structure

In the molecular orbital framework, based on the **linear combination of atomic orbitals** (LCAO), atomic orbitals combine to form molecular orbitals, which can be either **bonding** or **antibonding**.

In the case of **π bonds**, the bonding molecular orbitals are denoted as π, while the antibonding ones are denoted as π*.

The bonding π orbital has a lower energy and a symmetric electron density distribution between the atoms, whereas the antibonding π* orbital has higher energy and features a nodal plane between the atoms

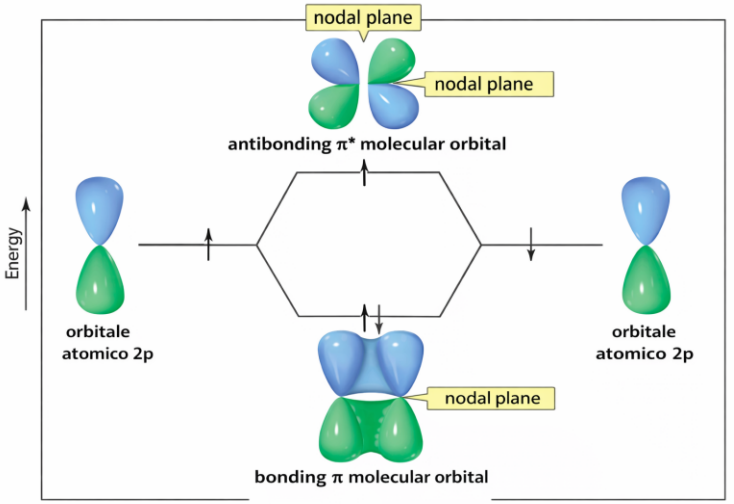

The same considerations apply to **σ bonds**.

σ bonds are responsible for the **structural stability of graphene**, while π bonds determine its **electronic properties**.

In particular, the following discussion will focus on the **band structure** of graphene, which originates from the overlap of π orbitals.

5.2 GRAPHENE

5.2.1 Crystal Structure

The structural properties of graphene are determined by sp^2 hybrid bonds arranged in a plane, with 120° angles between them, giving rise to a **hexagonal honeycomb lattice**.

To describe this structure, we introduce the concept of the **primitive cell**.

Although all carbon atoms are identical, we distinguish between two sublattices, labeled **A (blue)** and **B (yellow)**, so that each atom forms three bonds with atoms of the opposite color.

A pair of atoms, one from sublattice A and one from sublattice B, defines the basis of the primitive cell.

The primitive cell can then be constructed by considering, for each basis atom, an equilateral triangle formed with its nearest neighbors.

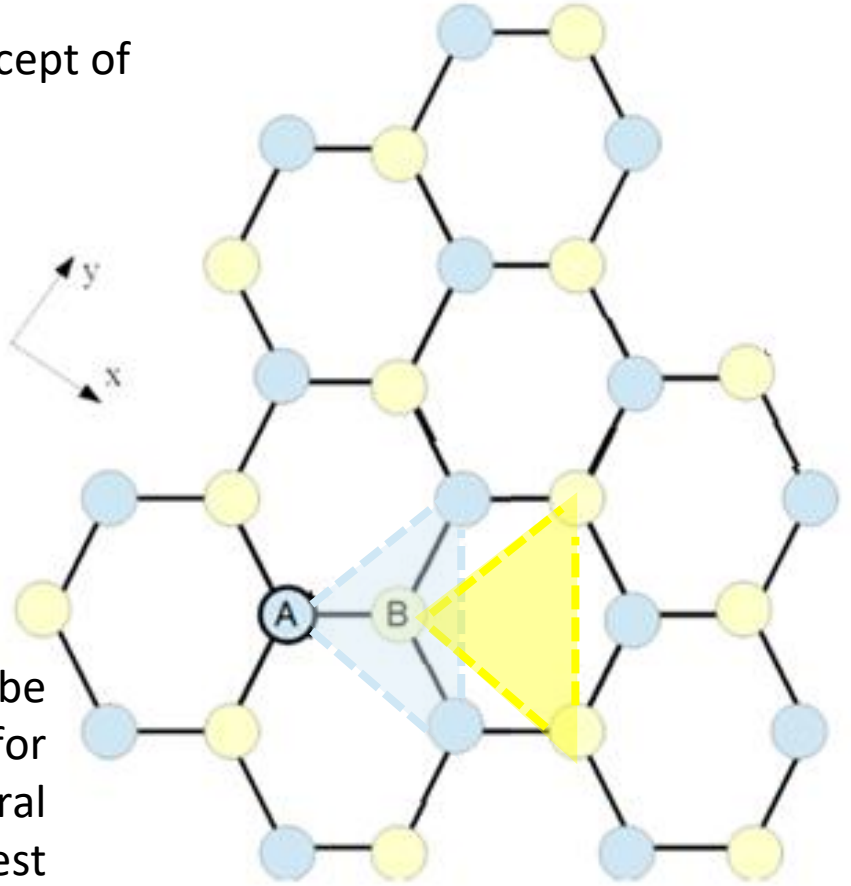

5.2 GRAPHENE

5.2.1 Crystal Structure

The honeycomb structure is not a Bravais lattice. Instead, it can be described as a **triangular Bravais lattice** with a basis of two carbon atoms, labeled A and B.

The primitive lattice vectors are denoted as $\overrightarrow{a_1}$ and $\overrightarrow{a_2}$, and they have the same magnitude.

Their length can be derived geometrically. If a_0 is the distance between nearest-neighbor carbon atoms, then:

$$|a_1| = 2a_0 sen60° = 2a_0 \frac{\sqrt{3}}{2} = a_0\sqrt{3} = |a_2|$$

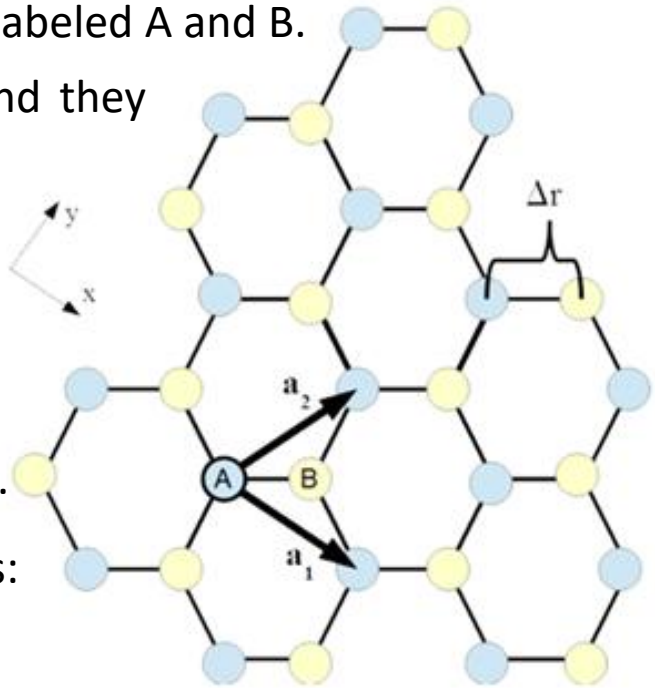

Each lattice point corresponds to two atoms, labeled A and B.

The position of an atom in sublattice A can be written as:

$$\overrightarrow{R_a} = n_1\overrightarrow{a_1} + n_2\overrightarrow{a_2}$$

Atoms in sublattice B are obtained by adding a displacement vector to the A sites:

$$\overrightarrow{R_b} = \overrightarrow{R_a} + \overrightarrow{\Delta r}$$

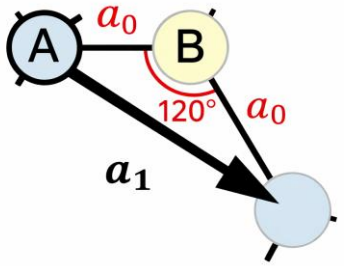

5.2 GRAPHENE

5.2.1 Crystal Structure

To simplify the description, we choose a Cartesian coordinate system such that the x-axis is aligned with $\overrightarrow{a_1}$. With this choice, the y-axis points toward the neighboring B atom.

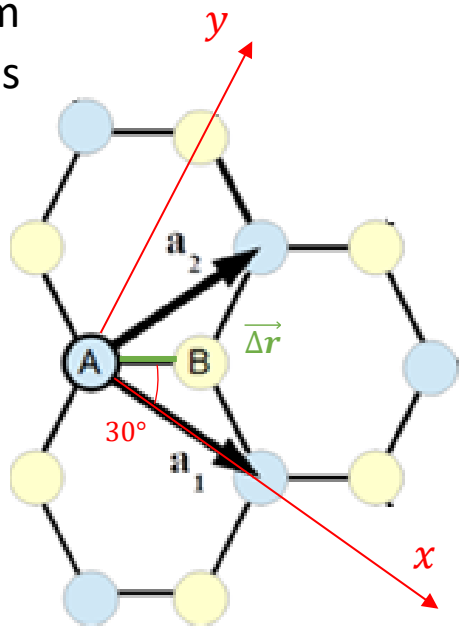

By expressing the primitive lattice vectors $\overrightarrow{a_1}$ and $\overrightarrow{a_2}$ in the Cartesian reference system, we obtain:

$$\overrightarrow{a_1} = \sqrt{3}a_0\widehat{u_x} \qquad \overrightarrow{a_2} = \frac{\sqrt{3}}{2}a_0\widehat{u_x} + \frac{3}{2}a_0\widehat{u_y}$$

We can also express the displacement vector $\overrightarrow{\Delta r}$ in component form:

$$\overrightarrow{\Delta r} = \frac{\sqrt{3}}{2}a_0\widehat{u_x} + \frac{1}{2}a_0\widehat{u_y}$$

By combining these expressions, we find a simple relation between $\overrightarrow{\Delta r}$ and the primitive vectors:

$$\overrightarrow{\Delta r} = \frac{1}{3}(\overrightarrow{a_1} + \overrightarrow{a_2})$$

$$|\overrightarrow{a_1}| = |\overrightarrow{a_2}| = a_0\sqrt{3}$$

$$|\overrightarrow{\Delta r}| = a_0$$

5.2 GRAPHENE

5.2.2 Brillouin Zone

The reciprocal lattice is defined by introducing vectors $\overrightarrow{A_1}$ and $\overrightarrow{A_2}$, such that:

$$\overrightarrow{a_i} \cdot \overrightarrow{A_j} = 2\pi\delta_{ij}$$

which implies:

$$\overrightarrow{a_1} \cdot \overrightarrow{A_1} = 2\pi \qquad \overrightarrow{a_1} \cdot \overrightarrow{A_2} = 0$$

$$\overrightarrow{a_2} \cdot \overrightarrow{A_1} = 0 \qquad \overrightarrow{a_2} \cdot \overrightarrow{A_2} = 2\pi$$

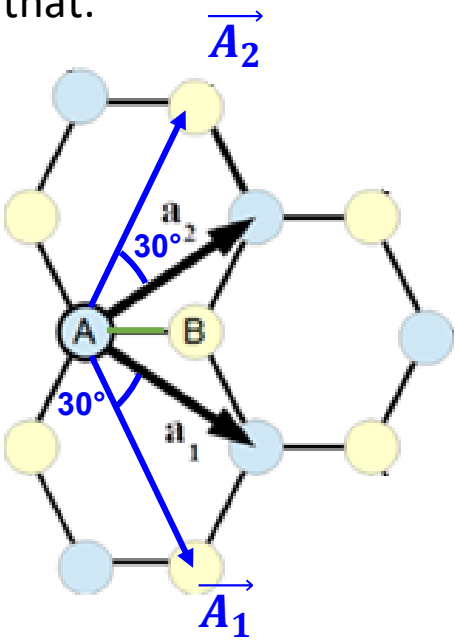

From these conditions, it follows that the reciprocal vectors are oriented such that $\overrightarrow{A_1}$ forms a 30° angle with $\overrightarrow{a_1}$, and $\overrightarrow{A_2}$ forms a 30° angle with $\overrightarrow{a_2}$.

If we rotate the reciprocal lattice vectors $\overrightarrow{A_1}$ and $\overrightarrow{A_2}$ by 30°, they point toward equivalent A sites.

Therefore, **the reciprocal lattice preserves the triangular Bravais structure of the direct lattice and is rotated by 30° with respect to it**.

5.2 GRAPHENE

5.2.2 Brillouin Zone

We can now construct the Brillouin zone of graphene, recalling that it is the **Wigner–Seitz cell of the reciprocal lattice**.

1. Start from a lattice point
2. Connect it to its nearest neighbors
3. Draw the perpendicular bisectors
4. The enclosed region is the Wigner–Seitz cell

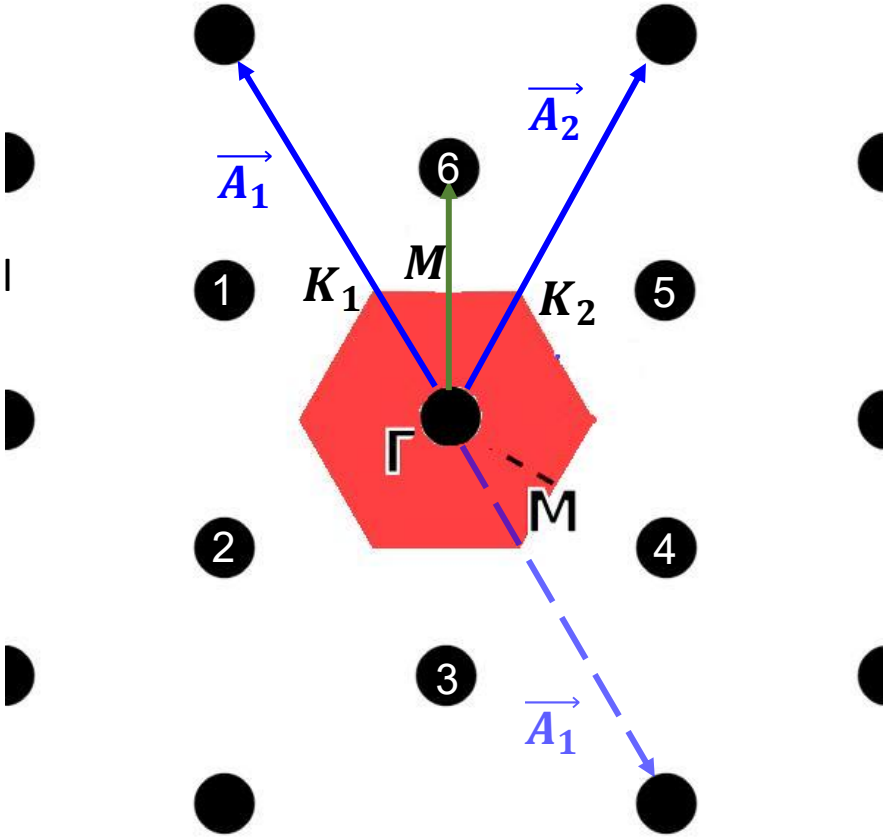

The center of the Brillouin zone is the Γ **point**, corresponding to zero wavevector.

The **high-symmetry directions** are:

$\Gamma - K_i$, where the K_i points are the vertices of the hexagon, known as **Dirac points**.

$\Gamma - M_i$, where the M_i points lie at the midpoints of the edges

5.2 GRAPHENE

5.2.3 Energy Bands - Tight Binding Method

To understand the basic electronic behavior of graphene, it is necessary to describe the behavior of its **π electrons**.

In the **tight-binding** model, each π electron is assumed to be tightly bound to its parent carbon atom, with only limited interaction with the potentials of neighboring atoms.

Let $\chi(\vec{r})$ be the wave function of the $2p_z$ atomic orbital of an isolated carbon atom. We denote by $\chi(\vec{r}-\vec{R})$ the corresponding wave function for a carbon atom located at the lattice site $\vec{R}$, where $\vec{r}$ is measured with respect to the origin of the coordinate system.

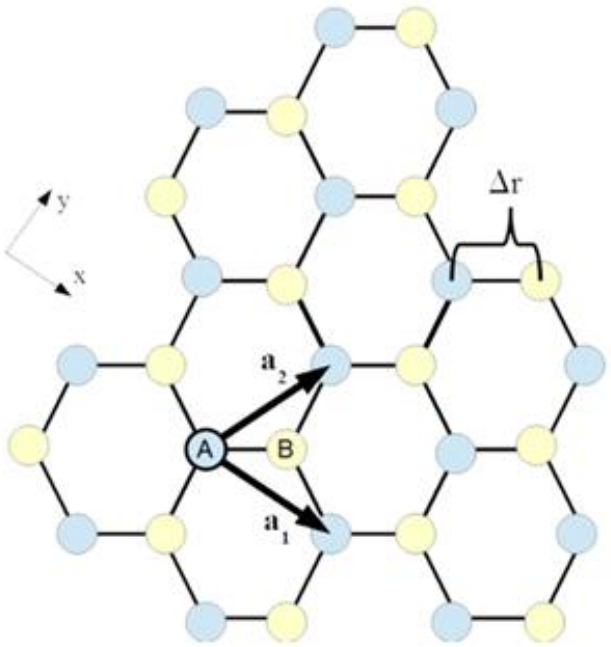

Since there are two atoms in each unit cell (at sites A and B), the π electronic wave function can be described using a two-dimensional basis. Each basis function is constructed from the atomic wave function $\chi(\vec{r}-\vec{R}_i)$, with $i = A$ or B, corresponding to the two sublattices.

5.2 GRAPHENE

5.2.3 Energy Bands - Tight Binding Method

Translational symmetry, as expressed by **Bloch's theorem**, together with the normalization of these basis functions in the tight-binding framework for graphene, leads to two basis wave functions that must satisfy Bloch's theorem:

$$|\phi_1\rangle = \frac{1}{\sqrt{N}} \sum_a e^{i\vec{k}\cdot\overrightarrow{R_a}} |\overrightarrow{R_a}\rangle \qquad |\phi_2\rangle = \frac{1}{\sqrt{N}} \sum_b e^{i\vec{k}\cdot\overrightarrow{R_b}} |\overrightarrow{R_b}\rangle$$

The eigenstates can be written as:

$$|\psi\rangle = \alpha|\phi_1\rangle + \beta|\phi_2\rangle$$

and must satisfy the Schrodinger equation:

$$\hat{H}|\psi\rangle = E|\psi\rangle$$

where $\hat{H}$ is the Hamiltonian of graphene and E is the single-electron energy.

If we now take the inner product of the Schrödinger equation with the basis functions $|\phi_1\rangle$ and $|\phi_2\rangle$, we obtain:

$$\langle\phi_1|\hat{H}|\psi\rangle = E\langle\phi_1|\psi\rangle \qquad \langle\phi_2|\hat{H}|\psi\rangle = E\langle\phi_2|\psi\rangle$$

5.2 GRAPHENE

5.2.3 Energy Bands - Tight Binding Method

$\langle\phi_1|\hat{H}|\psi\rangle = E\langle\phi_1|\psi\rangle$ $\langle\phi_2|\hat{H}|\psi\rangle = E\langle\phi_2|\psi\rangle$

Substituting: $|\psi\rangle = \alpha|\phi_1\rangle + \beta|\phi_2\rangle$

$$\alpha\langle\phi_1|\hat{H}|\phi_1\rangle + \beta\langle\phi_1|\hat{H}|\phi_2\rangle = \alpha E\langle\phi_1|\phi_1\rangle + \beta E\langle\phi_1|\phi_2\rangle$$

$$\alpha\langle\phi_2|\hat{H}|\phi_1\rangle + \beta\langle\phi_2|\hat{H}|\phi_2\rangle = \alpha E\langle\phi_2|\phi_1\rangle + \beta E\langle\phi_2|\phi_2\rangle$$

which can be written in matrix form as:

$$\begin{bmatrix} H_{11} & H_{12} \\ H_{21} & H_{22} \end{bmatrix}\begin{bmatrix}\alpha \\ \beta\end{bmatrix} = E\begin{bmatrix} S_{11} & S_{12} \\ S_{21} & S_{22} \end{bmatrix}\begin{bmatrix}\alpha \\ \beta\end{bmatrix}$$

where $H_{ij} = \langle\phi_i|\hat{H}|\phi_j\rangle$, $S_{ij} = \langle\phi_i|\phi_j\rangle$ with $i, j = 1,2$

Even though there are two distinct lattice sites, each carbon atom is identical to its neighbors. The energy of an electron in the $2p_z$ orbital of an isolated carbon atom is:

$$E_{2p_z} = \langle\phi_1|\hat{H}|\phi_1\rangle = \langle\phi_2|\hat{H}|\phi_2\rangle = H_{11} = H_{22}$$

5.2 GRAPHENE

5.2.3 Energy Bands - Tight Binding Method

$$\begin{bmatrix} H_{11} & H_{12} \\ H_{21} & H_{22} \end{bmatrix} \begin{bmatrix} \alpha \\ \beta \end{bmatrix} = E \begin{bmatrix} S_{11} & S_{12} \\ S_{21} & S_{22} \end{bmatrix} \begin{bmatrix} \alpha \\ \beta \end{bmatrix}$$

$$H_{ij} = \langle \phi_i | \hat{H} | \phi_j \rangle$$

$$S_{ij} = \langle \phi_i | \phi_j \rangle$$

The off-diagonal elements are related by the Hamiltonian $\hat{H}$ which must be **Hermitian**, therefore:

$$H_{12} = H_{21}^*$$

These elements correspond to the energy required for a π electron to "jump" from one lattice site to another (**hopping energy**).

If only nearest-neighbor hopping is considered, these off-diagonal elements take on a relatively simple form.

Let us choose a lattice site A as the origin, i.e., $\vec{R}_a = 0$.

We then consider the three nearest-neighbor lattice sites B to site A.

These are identified by the three vectors:

$$\overrightarrow{R_1} = \overrightarrow{\Delta r}$$

$$\overrightarrow{R_2} = \overrightarrow{\Delta r} - \overrightarrow{a_1}$$

$$\overrightarrow{R_3} = \overrightarrow{\Delta r} - \overrightarrow{a_2}$$

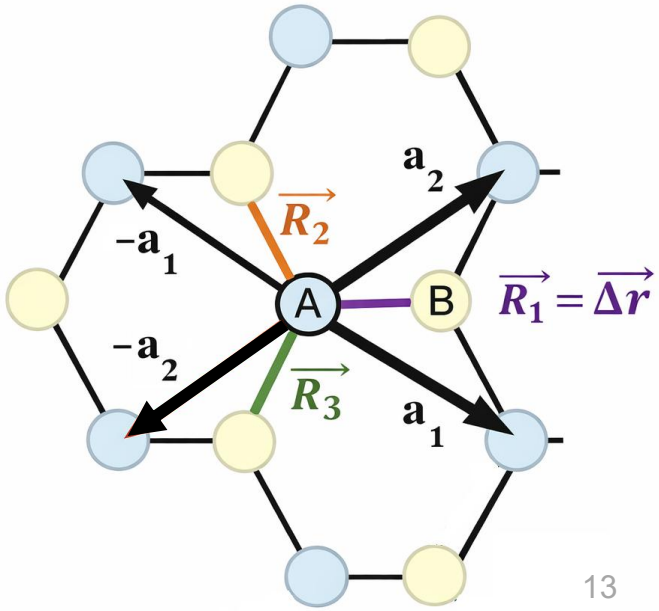

5.2 GRAPHENE

5.2.3 Energy Bands - Tight Binding Method

We now calculate the off-diagonal matrix element, whose general expression is given by:

$$H_{12} = \langle \phi_1 | \hat{H} | \phi_2 \rangle = \frac{1}{\sqrt{N}} \sum_a e^{i\vec{k}\cdot\overrightarrow{R_a}} \left\langle \overrightarrow{R_a} | \hat{H} \left| \left(\frac{1}{\sqrt{N}} \sum_b e^{i\vec{k}\cdot\overrightarrow{R_b}} | \overrightarrow{R_b} \rangle \right) \right. \right\rangle$$

$$|\phi_1\rangle = \frac{1}{\sqrt{N}} \sum_a e^{i\vec{k}\cdot\overrightarrow{R_a}} |\overrightarrow{R_a}\rangle$$

$$|\phi_2\rangle = \frac{1}{\sqrt{N}} \sum_b e^{i\vec{k}\cdot\overrightarrow{R_b}} |\overrightarrow{R_b}\rangle$$

If we restrict the summations to only the nearest neighbors of the lattice site A placed at the origin, we have $\overrightarrow{R_a} = 0$ and $e^{i\vec{k}\cdot\overrightarrow{R_a}} = 1$ while $b = 1,2,3$.

$$H_{12} = \frac{1}{\sqrt{N}} \left(\langle 0|\hat{H}|\overrightarrow{R_1}\rangle e^{i\vec{k}\cdot\overrightarrow{R_1}} + \langle 0|\hat{H}|\overrightarrow{R_2}\rangle e^{i\vec{k}\cdot\overrightarrow{R_2}} + \langle 0|\hat{H}|\overrightarrow{R_3}\rangle e^{i\vec{k}\cdot\overrightarrow{R_3}} \right)$$

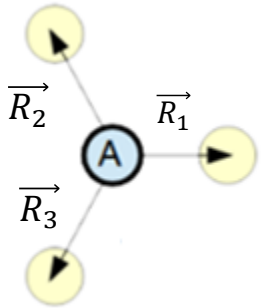

Assuming that:

$$\langle 0|\hat{H}|\overrightarrow{R_1}\rangle = \langle 0|\hat{H}|\overrightarrow{R_2}\rangle = \langle 0|\hat{H}|\overrightarrow{R_3}\rangle = -t$$

we obtain:

$$H_{12} = -\frac{1}{N} t \left(e^{i\vec{k}\cdot\overrightarrow{R_1}} + e^{i\vec{k}\cdot\overrightarrow{R_2}} + e^{i\vec{k}\cdot\overrightarrow{R_3}} \right)$$

$$\begin{bmatrix} H_{11} & H_{12} \\ H_{21} & H_{22} \end{bmatrix} \begin{bmatrix} \alpha \\ \beta \end{bmatrix} = E \begin{bmatrix} S_{11} & S_{12} \\ S_{21} & S_{22} \end{bmatrix} \begin{bmatrix} \alpha \\ \beta \end{bmatrix}$$

5.2 GRAPHENE

5.2.3 Energy Bands - Tight Binding Method

$$H_{12} = -\frac{1}{N} t \left(e^{i\vec{k}\cdot\overrightarrow{R_1}} + e^{i\vec{k}\cdot\overrightarrow{R_2}} + e^{i\vec{k}\cdot\overrightarrow{R_3}} \right)$$

This quantity t is called the **hopping integral** and represents the energy associated with electrons hopping between atoms. It is typically determined experimentally and is approximately $t \approx 2.75$ eV.

For the overlap integal matrix,

$$\begin{bmatrix} S_{11} & S_{12} \\ S_{21} & S_{22} \end{bmatrix}$$

its elements are determined in a similar way.

$$\begin{bmatrix} H_{11} & H_{12} \\ H_{21} & H_{22} \end{bmatrix} \begin{bmatrix} \alpha \\ \beta \end{bmatrix} = E \begin{bmatrix} S_{11} & S_{12} \\ S_{21} & S_{22} \end{bmatrix} \begin{bmatrix} \alpha \\ \beta \end{bmatrix}$$

$$H_{ij} = \langle \phi_i | \hat{H} | \phi_j \rangle$$

$$S_{ij} = \langle \phi_i | \phi_j \rangle$$

The overlap integral can be interpreted as a measure of the mutual similarity of the wave functions of two basis states:

$$S_{11} = S_{22} = \langle \phi_1 | \phi_1 \rangle = \langle \phi_2 | \phi_2 \rangle = 1$$

while, for the off-diagonal elements, the same steps and assumptions used for H_{12} are applied.

5.2 GRAPHENE

5.2.3 Energy Bands - Tight Binding Method

Therefore: $$S_{12} = \frac{1}{N} s \left(e^{i\vec{k}\cdot\overrightarrow{R_1}} + e^{i\vec{k}\cdot\overrightarrow{R_2}} + e^{i\vec{k}\cdot\overrightarrow{R_3}} \right)$$

$$H_{12} = -\frac{1}{N} t \left(e^{i\vec{k}\cdot\overrightarrow{R_1}} + e^{i\vec{k}\cdot\overrightarrow{R_2}} + e^{i\vec{k}\cdot\overrightarrow{R_3}} \right)$$

with: $$\langle 0|\overrightarrow{R_1}\rangle = \langle 0|\overrightarrow{R_2}\rangle = \langle 0|\overrightarrow{R_3}\rangle = s$$

The quantity s is also determined experimentally and is approximately $s \approx 0.13$.

Since $t \gg s$, to simplify the calculations we can assume $s \approx 0$and in this way the secular Schrodinger equation becomes:

$$\begin{bmatrix} E_{2p_z} & H_{12} \\ H_{12}^* & E_{2p_z} \end{bmatrix} \begin{bmatrix} \alpha \\ \beta \end{bmatrix} = E \begin{bmatrix} 1 & 0 \\ 0 & 1 \end{bmatrix} \begin{bmatrix} \alpha \\ \beta \end{bmatrix}$$

$$\begin{bmatrix} H_{11} & H_{12} \\ H_{21} & H_{22} \end{bmatrix} \begin{bmatrix} \alpha \\ \beta \end{bmatrix} = E \begin{bmatrix} S_{11} & S_{12} \\ S_{21} & S_{22} \end{bmatrix} \begin{bmatrix} \alpha \\ \beta \end{bmatrix}$$

$$E_{2p_z} = H_{11} = H_{22}$$

$$H_{21} = H_{12}^* = -\frac{1}{N} t \left(e^{-i\vec{k}\cdot\overrightarrow{R_1}} + e^{-i\vec{k}\cdot\overrightarrow{R_2}} + e^{-i\vec{k}\cdot\overrightarrow{R_3}} \right)$$

$$S_{12} = S_{21} = 0$$

$$S_{11} = S_{22} = 1$$

Let us impose that the determinant of the coefficient matrix is zero:

$$det \begin{bmatrix} E_{2p_z} - E & -t \left(e^{i\vec{k}\cdot\overrightarrow{R_1}} + e^{i\vec{k}\cdot\overrightarrow{R_2}} + e^{i\vec{k}\cdot\overrightarrow{R_3}} \right) \\ -t \left(e^{-i\vec{k}\cdot\overrightarrow{R_1}} + e^{-i\vec{k}\cdot\overrightarrow{R_2}} + e^{-i\vec{k}\cdot\overrightarrow{R_3}} \right) & E_{2p_z} - E \end{bmatrix} = 0$$

5.2 GRAPHENE

5.2.3 Energy Bands - Tight Binding Method

$$det\begin{bmatrix} E_{2p_z}-E & -t\left(e^{i\vec{k}\cdot\overrightarrow{R_1}}+e^{i\vec{k}\cdot\overrightarrow{R_2}}+e^{i\vec{k}\cdot\overrightarrow{R_3}}\right) \\ -t\left(e^{-i\vec{k}\cdot\overrightarrow{R_1}}+e^{-i\vec{k}\cdot\overrightarrow{R_2}}+e^{-i\vec{k}\cdot\overrightarrow{R_3}}\right) & E_{2p_z}-E \end{bmatrix}=0$$

Expanding the determinant:

$$0=E_{2pz}^2+E^2-2E_{2p_z}E-t^2\left(e^{i\vec{k}\cdot\overrightarrow{R_1}}+e^{i\vec{k}\cdot\overrightarrow{R_2}}+e^{i\vec{k}\cdot\overrightarrow{R_3}}\right)\left(e^{-i\vec{k}\cdot\overrightarrow{R_1}}+e^{-i\vec{k}\cdot\overrightarrow{R_2}}+e^{-i\vec{k}\cdot\overrightarrow{R_3}}\right)$$

We now expand the product using the expressions for $\overrightarrow{R_1}$, $\overrightarrow{R_2}$ and $\overrightarrow{R_3}$.

$$\overrightarrow{R_1}=\overrightarrow{\Delta r}$$
$$\overrightarrow{R_2}=\overrightarrow{\Delta r}-\overrightarrow{a_1}$$
$$\overrightarrow{R_3}=\overrightarrow{\Delta r}-\overrightarrow{a_2}$$

We note that terms with the same index satisfy:

$$e^{i\vec{k}\cdot\overrightarrow{R_i}}e^{-i\vec{k}\cdot\overrightarrow{R_i}}=1$$

while for different indices:

$$e^{i\vec{k}\cdot\overrightarrow{R_i}}e^{-i\vec{k}\cdot\overrightarrow{R_j}}=e^{i\vec{k}\cdot\left(\overrightarrow{R_i}-\overrightarrow{R_j}\right)}=e^{i\vec{k}\cdot\left(\overrightarrow{a_{i-1}}-\overrightarrow{a_{j-1}}\right)}$$

Thus, $\Delta\vec{r}$ cancels out in all terms, and we obtain:

$$0=E_{2pz}^2+E^2-2E_{2p_z}E-t^2\left(3+e^{i\vec{k}\cdot\overrightarrow{a_1}}+e^{i\vec{k}\cdot\overrightarrow{a_2}}+e^{-i\vec{k}\cdot\overrightarrow{a_1}}+\right.$$
$$\left.+e^{i\vec{k}\cdot\overrightarrow{a_2}-i\vec{k}\cdot\overrightarrow{a_1}}+e^{-i\vec{k}\cdot\overrightarrow{a_2}}+e^{i\vec{k}\cdot\overrightarrow{a_1}-i\vec{k}\cdot\overrightarrow{a_2}}\right)$$

5.2 GRAPHENE

5.2.3 Energy Bands - Tight Binding Method

$$0 = E_{2pz}^2 + E^2 - 2E_{2p_z}E - t^2\left(3 + e^{i\vec{k}\cdot\overrightarrow{a_1}} + e^{i\vec{k}\cdot\overrightarrow{a_2}} + e^{-i\vec{k}\cdot\overrightarrow{a_1}} + e^{i\vec{k}\cdot\overrightarrow{a_2}-i\vec{k}\cdot\overrightarrow{a_1}} + e^{-i\vec{k}\cdot\overrightarrow{a_2}} + e^{i\vec{k}\cdot\overrightarrow{a_1}-i\vec{k}\cdot\overrightarrow{a_2}}\right)$$

Using the expressions in Cartesian coodinates:

$$\overrightarrow{a_1} = \sqrt{3}a_0\widehat{u_x}$$

$$\overrightarrow{a_2} = \frac{\sqrt{3}}{2}a_0\widehat{u_x} + \frac{3}{2}a_0\widehat{u_x}$$

$$0 = E_{2pz}^2 + E^2 - 2E_{2p_z}E - t^2\left(3 + e^{i\sqrt{3}a_0k_x} + e^{i\frac{\sqrt{3}}{2}a_0k_x + i\frac{3}{2}a_0k_y}\right.$$
$$\left. + e^{-i\sqrt{3}a_0k_x} + e^{-i\frac{\sqrt{3}}{2}a_0k_x + i\frac{3}{2}a_0k_y} + e^{-i\frac{\sqrt{3}}{2}a_0k_x - i\frac{3}{2}a_0k_y} + e^{i\frac{\sqrt{3}}{2}a_0k_x - i\frac{3}{2}a_0k_y}\right)$$

The factor in round brackets in the characteristic equation can be expressed as:

$$3 + e^{i\sqrt{3}a_0k_x} + e^{-i\sqrt{3}a_0k_x} + e^{i\frac{\sqrt{3}}{2}a_0k_x + i\frac{3}{2}a_0k_y} + e^{-i\frac{\sqrt{3}}{2}a_0k_x + i\frac{3}{2}a_0k_y} + e^{-i\frac{\sqrt{3}}{2}a_0k_x - i\frac{3}{2}a_0k_y} + e^{i\frac{\sqrt{3}}{2}a_0k_x - i\frac{3}{2}a_0k_y}$$
$$= 3 + e^{i\sqrt{3}a_0k_x} + e^{-i\sqrt{3}a_0k_x} + \left(e^{i\frac{\sqrt{3}}{2}a_0k_x} + e^{-i\frac{\sqrt{3}}{2}a_0k_x}\right)\left(e^{i\frac{3}{2}a_0k_y} + e^{-i\frac{3}{2}a_0k_y}\right)$$

This is a second-degree equation whose solution is:

$$E = E_{2p_z} \pm t\sqrt{3 + 2cos\left(\sqrt{3}a_0k_x\right) + 4cos\left(\frac{\sqrt{3}}{2}a_0k_x\right)cos\left(\frac{3}{2}a_0k_y\right)}$$

5.2 GRAPHENE

5.2.3 Energy Bands - Tight Binding Method

$$E = E_{2p_z} \pm t\sqrt{3 + 2cos\left(\sqrt{3}a_0k_x\right) + 4cos\left(\frac{\sqrt{3}}{2}a_0k_x\right)cos\left(\frac{3}{2}a_0k_y\right)}$$

It is common to set this reference energy to approximately zero, where the "+" solution corresponds to the antibonding state and the "−" solution to the bonding state.

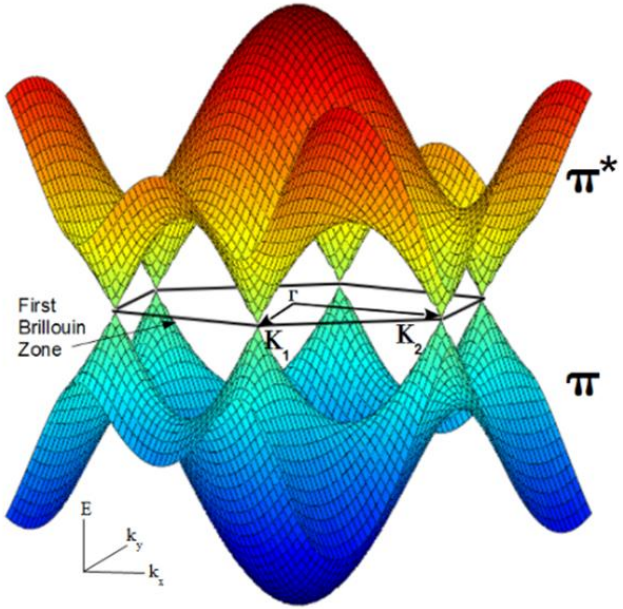

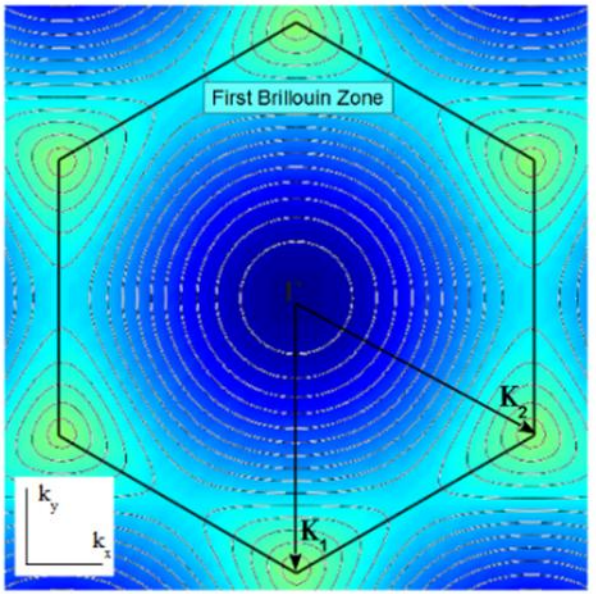

Referring to the Figure, note that these two energies are degenerate only at specific points corresponding to the minimum energy.

5.2 GRAPHENE

5.2.3 Energy Bands - Tight Binding Method

$$E = E_{2p_z} \pm \sqrt{3 + 2cos(\sqrt{3}a_0k_x) + 4cos\left(\frac{\sqrt{3}}{2}a_0k_x\right)cos\left(\frac{3}{2}a_0k_y\right)}$$

Near the low-energy points (Dirac points), it can be shown that the energy bands can be approximated by conical dispersions for both states.

It can be shown that the dispersion relation in the low energy limit can be approximated by:

$$E = E_{2p_z} \pm \frac{3}{2}a_0t\sqrt{\Delta k_x^2 + \Delta k_y^2} = E_{2p_z} \pm \frac{3}{2}a_0t|\Delta k|$$

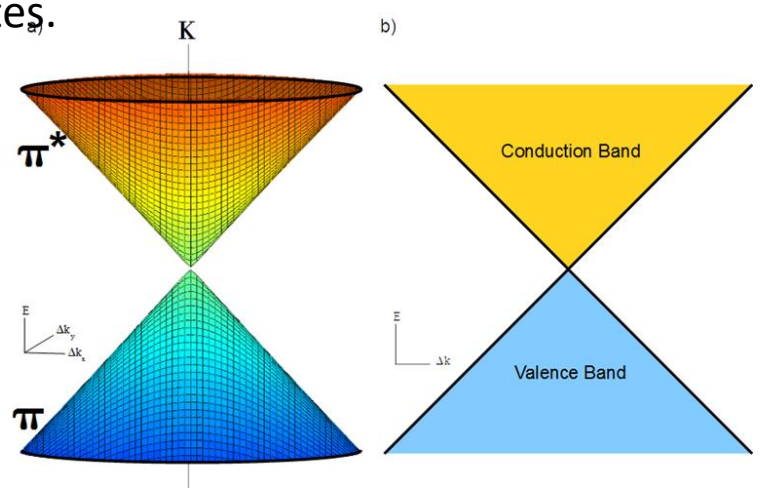

For this reason, graphene is a **zero-band-gap** semiconductor.

Knowing the energy dispersion provides a direct relationship with the frequency and the group velocity, defined as:

$$\omega = \frac{E}{\hbar}$$

$$v = \frac{d\omega}{dk} = \frac{1}{\hbar}\frac{dE}{dk} = \frac{3}{2\hbar}a_0t$$

5.2 GRAPHENE

5.2.3 Energy Bands - Tight Binding Method

Substituting $a_0 \approx 1.42 \times 10^{-10}$ m and $t \approx 2.75$ eV $\simeq 4.4 \times 10^{-19}$ J:

$$v = \frac{3}{2\hbar} a_0 t$$

$$v = \frac{3}{2\hbar} a_0 t = \frac{3}{2 \cdot 1.055 \times 10^{-34}} (1.42 \times 10^{-10})(4.4 \times 10^{-19}) \approx 1.0 \times 10^6 \text{ m/s}$$

$$v \approx \frac{1}{300} c$$

where c is the speed of light. This value is of the **same order of magnitude as in metals**.

We can rewrite the dispersion relation as:

$$E = E_{2p_z} \pm \frac{3}{2} a_0 t |\Delta k|$$

$$E = E_{2p_z} \pm v\hbar\Delta k$$

The Fermi energy will be: $E_F = v\hbar k_F$

A linear dispersion also leads to a **linear density of states**.

The volume of states in momentum space is:

$$V_k = \pi k^2$$

so that the volume of a shell between k and $k + dk$ is:

$$dV_k = 2\pi k dk$$

5.2 GRAPHENE

5.2.4 Density of states

The volume associated with a single state in k-space is:

$$\frac{4\pi^2}{V_0}$$

Then, the number of single-electron states is given by the ratio between the total volume in the region between k and $k + dk$ and the volume of a single state:

$$dN = 4\frac{2\pi k dk}{4\pi^2 V_0^{-1}} = \frac{2V_0 k dk}{\pi}$$

$dV_k = 2\pi k dk$

where the factor 4 accounts for both spin and valley degeneracy.

In terms of energy: $\frac{dk}{dE} = \frac{1}{v\hbar}$

$E = E_{2p_z} \pm v\hbar\Delta k$

The number of states will be: $dN = \frac{2V_0}{\pi} k \frac{dk}{dE} dE = \frac{2V_0 E}{\pi\hbar^2 v^2} dE$

Therefore, the density of states per unit energy and volume is:

$$D(E) = \frac{1}{V_0}\frac{dN}{dE} = \frac{2E}{\pi v^2 \hbar^2}$$

Thus, **the density of states increases linearly with energy**.

5.3 QUANTUM WIRE

5.3.1 Energy bands

Quantum wire structures confine the motion of electrons in the conduction band in two dimensions (x and y), while they remain free to move along the z direction.

Exactly as we did for 2D structures—where we first considered a heterostructure with alternating semiconductors in a plane and then a graphene sheet—here we will follow the same approach: we will first consider a **quantum wire grown on a substrate**, modeled as a rectangular rod, and then an **ideal quantum wire**.

A convenient way to treat a quantum wire mathematically is to start from the results obtained for a quantum well, where confinement in the x direction has already been considered, and then introduce **confinement in the second direction (y)**.

This is not the only way to model a quantum wire, and it does not provide fully general expressions for wave functions and energies, but it is useful for gaining physical insight.

The simplest geometry we can consider is a **rectangular bar surrounded by infinite potential barriers**.

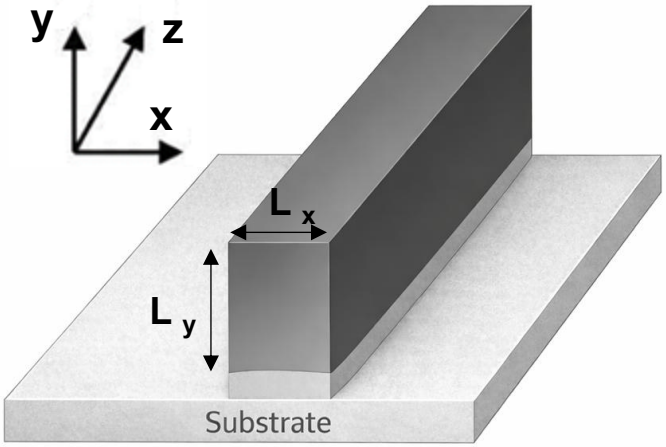

5.3 QUANTUM WIRE

5.3.1 Energy bands

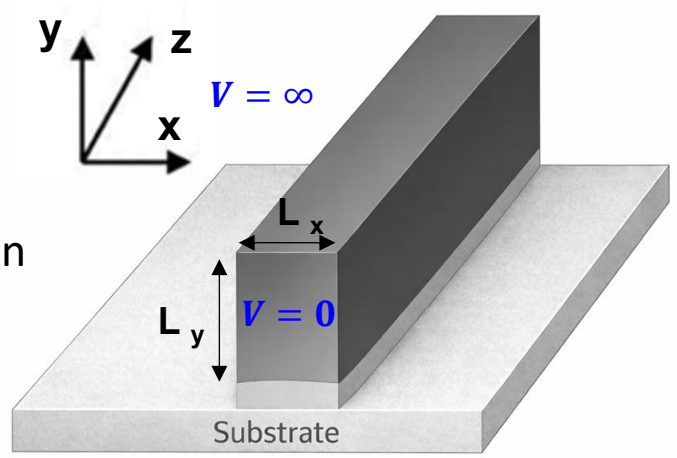

Inside the quantum wire, the potential is zero, while outside it is infinite.

Therefore, the wave function outside the quantum wire can be assumed to be zero.

The total wave function can be written as the product of two components:

$$\Psi(x,y,z) = \Psi_z(z)\Psi(x,y)$$

Only the wave function along the z direction can be expressed as a plane wave:

$$\Psi_z(z) = Ae^{ik_z z}$$

where A is the normalization constant.

The **Schrödinger equation** inside the quantum wire for motion in the two confined directions is:

$$-\frac{\hbar^2}{2m^*}\left[\frac{\partial^2\Psi(x,y)}{\partial x^2} + \frac{\partial^2\Psi(x,y)}{\partial y^2}\right] = E_{x,y}\,\Psi(x,y)$$

5.3 QUANTUM WIRE

5.3.1 Energy bands

The separation of variables in the Schrödinger equation allows us to factorize the wave function as:

$$\Psi(x,y) = \Psi(x)\Psi(y)$$

and the equation becomes:

$$-\frac{\hbar^2}{2m^*}\Psi(y)\frac{\partial^2\Psi(x)}{\partial x^2} - \frac{\hbar^2}{2m^*}\Psi(x)\frac{\partial^2\Psi(y)}{\partial y^2} = \left(E_x + E_y\right)\Psi(x)\Psi(y)$$

where the energy has been separated into two contributions:

$$E_{x,y} = E_x + E_y$$

The equation can then be separated into two independent equations:

$$-\frac{\hbar^2}{2m^*}\frac{\partial^2\Psi(x)}{\partial x^2} = E_x\Psi(x) \qquad -\frac{\hbar^2}{2m^*}\frac{\partial^2\Psi(y)}{\partial y^2} = E_y\Psi(y)$$

These are the same equations as for an infinite potential well . The solutions are:

$$\Psi(x) = \sqrt{\frac{2}{L_x}}sen\left(\frac{\pi n x}{L_x}\right) \qquad \Psi(y) = \sqrt{\frac{2}{L_y}}sen\left(\frac{\pi m y}{L_y}\right)$$

5.3 QUANTUM WIRE

5.3.1 Energy bands

Their corresponding energies are:

$$(\mathrm{E}_x)_n = \frac{\hbar^2 (k_x^2)_n}{2m^*} = \frac{\hbar^2 \pi^2 n^2}{2m^* L_x^2}$$

$$\left(\mathrm{E}_y\right)_m = \frac{\hbar^2 \left(k_y^2\right)_m}{2m^*} = \frac{\hbar^2 \pi^2 m^2}{2m^* L_y^2}$$

The total energy is therefore the sum of three contributions:

$$E(k_z, n, m) = \mathrm{E}_z(k_z) + (\mathrm{E}_x)_n + \left(\mathrm{E}_y\right)_m = \frac{\hbar^2 k_z^2}{2m^*} + \frac{\hbar^2 (k_x^2)_n}{2m^*} + \frac{\hbar^2 \left(k_y^2\right)_m}{2m^*}$$

where n and m are integers that label the quantized energy levels $(E_x)_n$ and $\left(E_y\right)_m$, as well as the corresponding quantized wave numbers $(k_x)_n$ and $\left(k_y\right)_m$, resulting from the confinement of electron motion in the x and y direction, respectively.

The values of $(E_x)_n$and $\left(E_y\right)_m$can be determined more accurately by solving the finite potential well problem.

5.3 QUANTUM WIRE

5.3.2 Density of states

The density of states of electrons in the conduction band is given by:

$$g_{1D}(E) = 2 \sum_{n,m,k_z} \delta\left[\mathrm{E}_z(k_z) + (\mathrm{E}_x)_n + \left(\mathrm{E}_y\right)_m - E\right]$$

Since k_z is continuous, the sum can be replaced by an integral:

$$\sum_{k_z} \rightarrow \frac{L}{2\pi} \int dk_z$$

$$E(k_z, n, m) = \mathrm{E}_z(k_z) + (\mathrm{E}_x)_n + \left(\mathrm{E}_y\right)_m$$

where $\frac{2\pi}{L}$ is the length of a single state in 1D k-space, and L is the length of the quantum wire in the real space.

Therefore, we can rewrite $g_{1D}(E)$as:

$$g_{1D}(E) = \frac{L}{\pi} \sum_{n,m} \int_0^{+\infty} \delta\left[\mathrm{E}_z(k_z) + (\mathrm{E}_x)_n + \left(\mathrm{E}_y\right)_m - E\right] dk_z$$

Proceeding as in the case of 2D heterostructures:

$$\mathrm{E}_z(k_z) = \frac{\hbar^2 k_z^2}{2m^*}$$

$$d[\mathrm{E}_z(k_z)] = \frac{\hbar^2}{m^*} k_z dk_z = \frac{\hbar^2}{m^*} \sqrt{\frac{2m^* \mathrm{E}_z(k_z)}{\hbar^2}}\, dk_z$$

5.3 QUANTUM WIRE

5.3.2 Density of states

$$g_{1D}(E) = \frac{L}{\pi}\sum_{n,m}\int_0^{+\infty} \delta\left[\mathrm{E}_z(k_z) + (\mathrm{E}_x)_n + (\mathrm{E}_y)_m - E\right] dk_z$$

$$d[\mathrm{E}_z(k_z)] = \frac{\hbar^2}{m^*}\sqrt{\frac{2m^*\mathrm{E}_z(k_z)}{\hbar^2}}\,dk_z$$

Substituting:

$$g_{1D}(E) = \frac{L}{\pi\hbar}\sqrt{\frac{m^*}{2}}\sum_{n,m}\int_0^{+\infty} \delta\left[\mathrm{E}_z(k_z) + (\mathrm{E}_x)_n + (\mathrm{E}_y)_m - E\right]\frac{1}{\sqrt{\mathrm{E}_z(k_z)}}\,d\mathrm{E}_z$$

The integral can be evaluated using the property of the Dirac delta function,

$$\int_0^{+\infty} \delta(x - x_0)\, f(x)\, dx = \begin{cases} f(x_0), & x_0 > 0 \\ 0, & x_0 < 0 \end{cases}$$

In a compact way, it can be written as

$$\int_0^{+\infty} \delta(x - x_0)\, f(x)\, dx = \Theta(x_0)\, f(x_0)$$

$$\Theta(\mathrm{x}) := \int_{-\infty}^{x} \delta(s)ds$$

Applying in our case in which $x_0 = E - \left((\mathrm{E}_x)_n + (\mathrm{E}_y)_m\right)$ and $x = \mathrm{E}_z$, we obtain:

$$g_{1D}(E) = \frac{L}{\pi\hbar}\sqrt{\frac{m^*}{2}}\sum_{n,m}\frac{\Theta\left[E - \left[(\mathrm{E}_x)_n + (\mathrm{E}_y)_m\right]\right]}{\sqrt{E - \left[(\mathrm{E}_x)_n + (\mathrm{E}_y)_m\right]}}$$

5.3 QUANTUM WIRE

5.3.2 Density of states

$$g_{1D}(E) = \frac{L}{\pi\hbar}\sqrt{\frac{m^*}{2}}\sum_{n,m}\frac{\Theta\left[E - \left[(\mathrm{E}_x)_n + (\mathrm{E}_y)_m\right]\right]}{\sqrt{E - \left[(\mathrm{E}_x)_n + (\mathrm{E}_y)_m\right]}}$$

$$E(k_z, n, m) = \frac{\hbar^2 k_z^2}{2m^*} + (\mathrm{E}_x)_n + (\mathrm{E}_y)_m$$

With respect to 2D heterostructures, instead of a single quantum number n, we have a **set of discrete levels labeled by two indices** (n, m) for the in-plane confinement.

For each transverse level, the energy dispersion is:

$$E_{n,m}(k_z) = E_{n,m} + \frac{\hbar^2 k_z^2}{2m^*} \qquad \text{with} \quad E_{n,m} = (E_x)_n + (E_y)_m$$

Thus, the spectrum consists of multiple **parabolic subbands**, each shifted upward by the corresponding transverse energy $E_{n,m}$.

This is analogous to the 2D case; however, while in that case each parabola is labeled by a single index n, here they are labeled by the pair (n, m).

Conversely, the density of states differs significantly from the 2D case.

Each subband contributes a term of the form: $g_{1D}(E) \propto \frac{1}{\sqrt{E - E_{n,m}}}$

5.3 QUANTUM WIRE

5.3.2 Density of states

$$E_{n,m}(k_z) = E_{n,m} + \frac{\hbar^2 k_z^2}{2m^*}$$

$$g_{1D}(E) \propto \sum_{n,m} \frac{1}{\sqrt{E - E_{n,m}}}$$

Instead of the step-like behavior in 2D systems, the density of states exhibits divergences. These divergences occur at energies where E coincides with the bottom of each subband $E_{n,m}$, giving rise to the so-called **Van Hove singularities**.

Instead of steps, the density of states is characterized by a series of sharp peaks, each associated with a different pair of quantum numbers (n, m).

These singularities arise within the idealized model. In real systems, peaks remain finite due to effects such as electron–electron interactions.

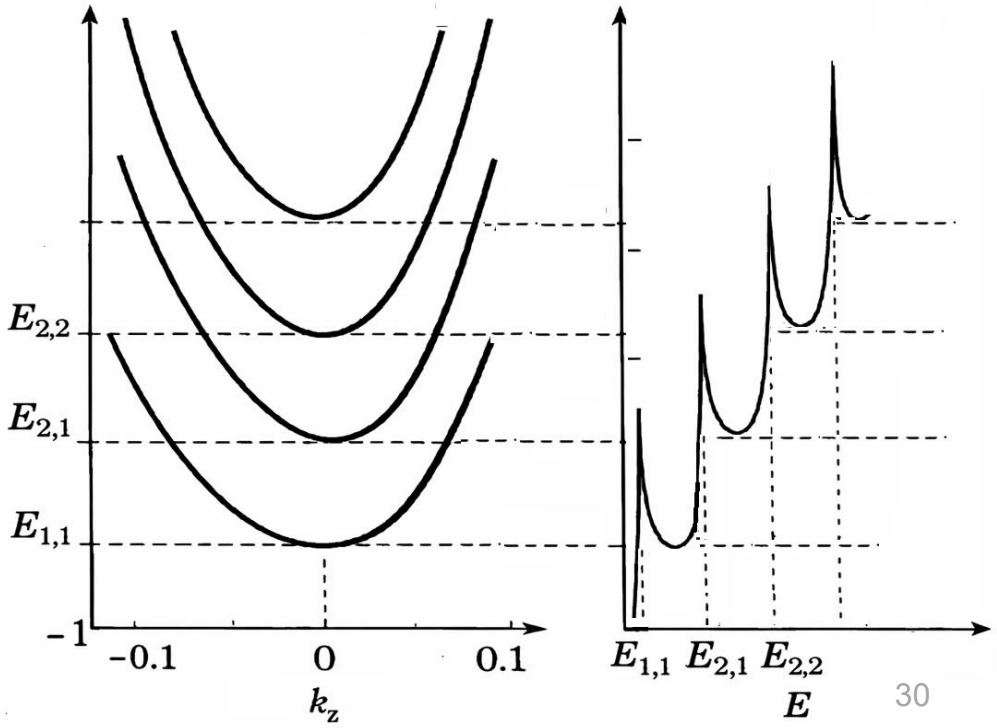

5.3 QUANTUM WIRE

5.3.3 GaAs Nanowire : Subbands and probability density

In the previous discussion, we considered a quantum wire grown on a semiconductor substrate and modeled it as a rectangular rod. Here, we will instead consider an **ideal nanowire**, treated as a true one-dimensional system.

Consider an infinitely long, cylindrically symmetric nanowire of radius R.

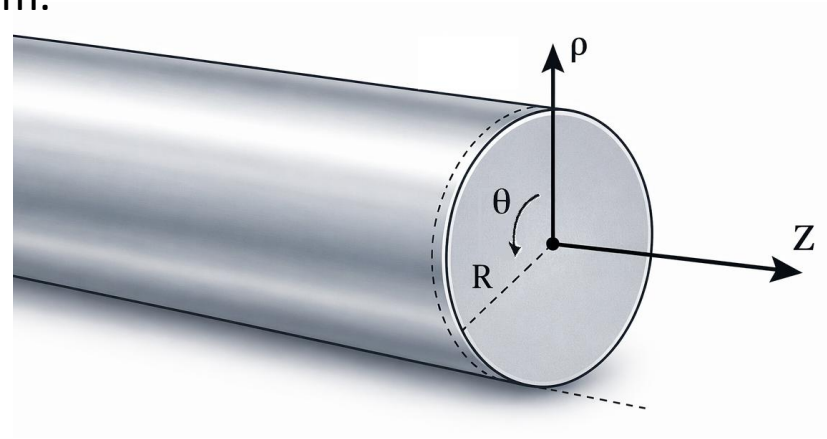

Let us start from the Schrödinger equation in the effective mass approximation:

$$\left[-\frac{\hbar^2}{2m^*}\nabla^2 + \mathrm{V}(\vec{r})\right]\Psi(\vec{r}) = E\Psi(\vec{r})$$

where $V(\vec{r})$ is the potential, $\Psi(\vec{r})$ is the electron eigenstate, and E is the energy eigenvalue measured from the bottom of the conduction band.

Given the geometry of the problem, it is convenient to rewrite the Schrödinger equation in **cylindrical coordinates**.

We introduce the cylindrical coordinates ρ, θ, and z, as shown in the Figure.

5.3 QUANTUM WIRE

5.3.3 GaAs Nanowire : Subbands and probability density

The relations between cylindrical and Cartesian coordinates are:

$$\begin{cases} x = \rho cos\theta \\ y = \rho sen\theta \\ z = z \end{cases} \quad \text{with:} \quad \begin{matrix} \rho \in [0, R] \\ \theta \in [0, 2\pi] \end{matrix}$$

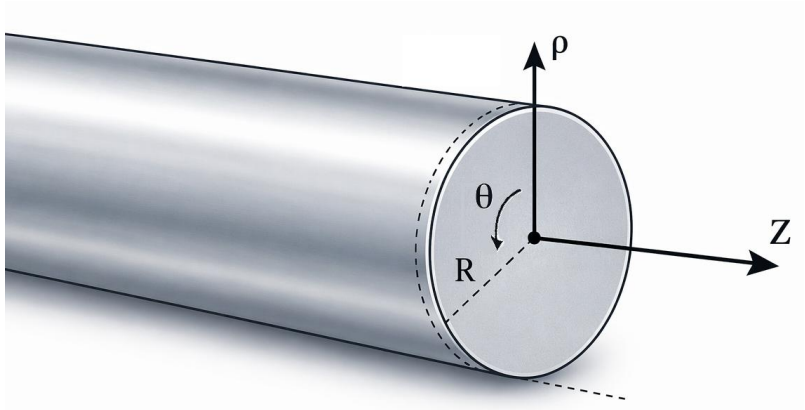

To rewrite the Schrödinger equation in cylindrical coordinates, it is sufficient to express the Laplacian operator ∇^2 in cylindrical form:

$$\left[-\frac{\hbar^2}{2m^*}\nabla^2 + \mathrm{V}(\vec{r})\right]\Psi(\vec{r}) = E\Psi(\vec{r})$$

$$\nabla^2 = \frac{\partial^2}{\partial x^2} + \frac{\partial^2}{\partial y^2} + \frac{\partial^2}{\partial z^2} = \frac{1}{\rho}\frac{\partial}{\partial \rho}\left(\rho\frac{\partial}{\partial \rho}\right) + \frac{1}{\rho^2}\frac{\partial^2}{\partial \theta^2} + \frac{\partial^2}{\partial z^2}$$

As in the case of a rectangular cross-section nanowire, we assume that the potential is zero inside the nanowire and infinite outside.

Accordingly, we impose the boundary condition that $\Psi(\vec{r})$ vanishes at the surface of the nanowire.

5.3 QUANTUM WIRE

5.3.3 GaAs Nanowire : Subbands and probability density

The separation of variables in the Schrödinger equation allows us to separate the contributions $\Psi(\rho,\theta,z)$ of associated with the cylindrical coordinates, namely:

$$\Psi(\rho,\theta,z) = u(\rho)\Theta(\theta)Z(z)$$

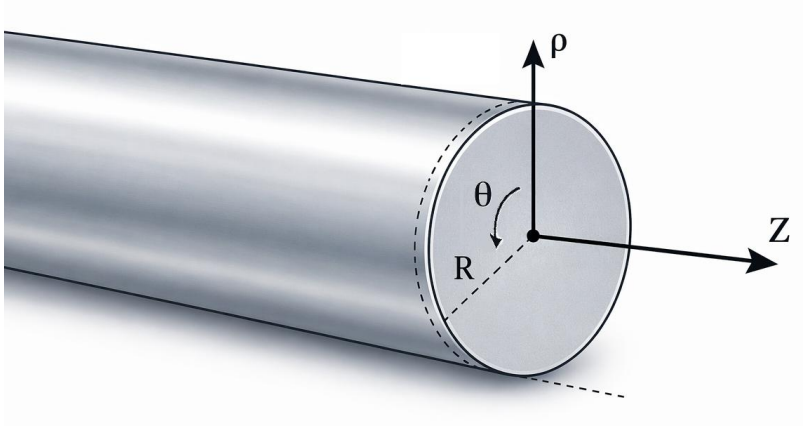

Since the nanowire is infinitely long, we can assume plane-wave solutions along the z direction:

$$Z(z) = e^{ik_z z}$$

$$\left[-\frac{\hbar^2}{2m^*}\nabla^2 + \mathrm{V}(\vec{r})\right]\Psi(\vec{r}) = E\Psi(\vec{r})$$

where k_z is the wavenumber along the direction z and is a continuous variable.

The Schrodinger equation in cylindrical coordinates take the form:

$$-\frac{\hbar^2}{2m^*}\left[\frac{1}{\rho}\frac{\partial}{\partial\rho}\left(\rho\frac{\partial\Psi}{\partial\rho}\right) + \frac{1}{\rho^2}\frac{\partial^2\Psi}{\partial\theta^2} + \frac{\partial^2\Psi}{\partial z^2}\right] = E\Psi$$

5.3 QUANTUM WIRE

5.3.3 GaAs Nanowire : Subbands and probability density

$$-\frac{\hbar^2}{2m^*}\left[\frac{1}{\rho}\frac{\partial}{\partial\rho}\left(\rho\frac{\partial\Psi(\vec{r})}{\partial\rho}\right)+\frac{1}{\rho^2}\frac{\partial^2\Psi(\vec{r})}{\partial\theta^2}+\frac{\partial^2\Psi(\vec{r})}{\partial z^2}\right]=E\Psi(\vec{r})$$

$$\Psi(\vec{r})=u(\rho)\Theta(\theta)Z(z)$$

$$Z(z)=e^{ik_z z}$$

Let us compute the derivatives in the Schrödinger equation term by term:

$$\frac{1}{\rho}\frac{\partial}{\partial\rho}\left(\rho\frac{\partial\Psi(\vec{r})}{\partial\rho}\right)=\frac{1}{\rho}\frac{\partial}{\partial\rho}[\rho u'(\rho)\Theta(\theta)Z(z)]=\frac{1}{\rho}u'(\rho)\Theta(\theta)Z(z)+u''(\rho)\Theta(\theta)Z(z)$$

$$\frac{1}{\rho^2}\frac{\partial^2\Psi(\vec{r})}{\partial\theta^2}=\frac{1}{\rho^2}u(\rho)\Theta''(\theta)Z(z)$$

$$\frac{\partial^2\Psi(\vec{r})}{\partial z^2}=-u(\rho)\Theta(\theta)Z(z)k_z^2$$

Substituting these expressions, we obtain:

$$-\frac{\hbar^2}{2m^*}\left[\frac{1}{\rho}u'(\rho)\Theta(\theta)Z(z)+u''(\rho)\Theta(\theta)Z(z)+\frac{1}{\rho^2}u(\rho)\Theta''(\theta)Z(z)-u(\rho)\Theta(\theta)Z(z)k_z^2\right]=Eu(\rho)\Theta(\theta)Z(z)$$

5.3 QUANTUM WIRE

5.3.3 GaAs Nanowire : Subbands and probability density

$$-\frac{\hbar^2}{2m^*}\left[\frac{1}{\rho}u'(\rho)\Theta(\theta)Z(z)+u''(\rho)\Theta(\theta)Z(z)+\frac{1}{\rho^2}u(\rho)\Theta''(\theta)Z(z)-u(\rho)\Theta(\theta)Z(z)k_z^2\right]=Eu(\rho)\Theta(\theta)Z(z)$$

We divide both sides by $u(\rho)\Theta(\theta)Z(z)$ and obtain:

$$\frac{1}{\rho}\frac{u'(\rho)}{u(\rho)}+\frac{u''(\rho)}{u(\rho)}+\frac{1}{\rho^2}\frac{\Theta''(\theta)}{\Theta(\theta)}-k_z^2=-\frac{2m^*E}{\hbar^2}$$

Multiplying both sides by ρ^2 we obtain:

$$\rho^2\frac{u''(\rho)}{u(\rho)}+\rho\frac{u'(\rho)}{u(\rho)}+\frac{\Theta''(\theta)}{\Theta(\theta)}=\left(k_z^2-\frac{2m^*E}{\hbar^2}\right)\rho^2$$

Using the method of separation of variables, we conclude that each side must be equal to a constant C, independent of both θ and ρ:

$$\rho^2\frac{u''(\rho)}{u(\rho)}+\rho\frac{u'(\rho)}{u(\rho)}-\left(k_z^2-\frac{2m^*E}{\hbar^2}\right)\rho^2=-\frac{\Theta''(\theta)}{\Theta(\theta)}=C$$

Let us first solve the angular differential equation for $\Theta(\theta)$:

$$\Theta''(\theta)+C\Theta(\theta)=0$$

5.3 QUANTUM WIRE

5.3.3 GaAs Nanowire : Subbands and probability density

$$\rho^2\frac{u''(\rho)}{u(\rho)}+\rho\frac{u'(\rho)}{u(\rho)}-\left(k_z^2-\frac{2m^*E}{\hbar^2}\right)\rho^2=-\frac{\Theta''(\theta)}{\Theta(\theta)}=C$$

$$\Theta''(\theta)+C\Theta(\theta)=0$$

The general solution is:

$$\Theta(\theta)=\mathrm{A}e^{i\sqrt{C}\theta}+\mathrm{B}e^{-i\sqrt{C}\theta}$$

To satisfy the 2π-periodicity of θ, we must impose:

$$\Theta(0)=\Theta(2\pi)$$

which is satisfied only if $\sqrt{C}$ is an integer.

We therefore introduce an integer l such that $l^2=C$, and the angular solution becomes:

$$\Theta(\theta)=\mathrm{A}e^{il\theta}+\mathrm{B}e^{-il\theta} \qquad \text{with} \quad l=0,\pm1,\pm2\ldots$$

where l can be interpreted as the **angular momentum quantum number**.

We now turn to the radial differential equation for $u(\rho)$

$$\rho^2\frac{u''(\rho)}{u(\rho)}+\rho\frac{u'(\rho)}{u(\rho)}-\left(k_z^2-\frac{2m^*E}{\hbar^2}\right)\rho^2=C=l^2$$

5.3 QUANTUM WIRE

5.3.3 GaAs Nanowire : Subbands and probability density

$$\rho^2 \frac{u''(\rho)}{u(\rho)} + \rho \frac{u'(\rho)}{u(\rho)} - \left(k_z^2 - \frac{2m^* E}{\hbar^2}\right)\rho^2 = l^2$$

Let us introduce:

$$\mathcal{E} = E - \frac{\hbar^2 k_z^2}{2m^*}$$

and rewrite the equation (dividing both sides by ρ^2):

$$u''(\rho) + \frac{u'(\rho)}{\rho} + \left(\frac{2m^*\mathcal{E}}{\hbar^2} - \frac{l^2}{\rho^2}\right)u(\rho) = 0$$

$$\frac{d^2y}{dx^2} + \frac{1}{x}\frac{dy}{dx} + \left(1 \pm \frac{\alpha^2}{x^2}\right)y = 0$$

This is the Bessel differential equation in the variable $x = \sqrt{\frac{2m^*\mathcal{E}}{\hbar^2}}\rho$ e $\alpha = l$.

The solutions are the Bessel cylindrical functions:

$$u(\rho) = aJ_l\left(\sqrt{\frac{2m^*\mathcal{E}}{\hbar^2}}\rho\right)$$

5.3 QUANTUM WIRE

5.3.3 GaAs Nanowire : Subbands and probability density

The electron wave function in a nanowire can therefore be written as:

$$\Psi(\vec{r}) = aJ_l\left(\sqrt{\frac{2m^*\mathcal{E}}{\hbar^2}}\rho\right)\left(\mathrm{A}e^{il\theta} + \mathrm{B}e^{-il\theta}\right)e^{ik_z z}$$

We have not yet imposed the boundary condition that the wave function must vanish at the surface of the nanowire, i.e., $u(R) = 0$.

This condition is equivalent to requiring that the Bessel function vanishes at $\rho = R$.

For each value of l, the Bessel function has an **infinite discrete set of zeros**, which we index by n.

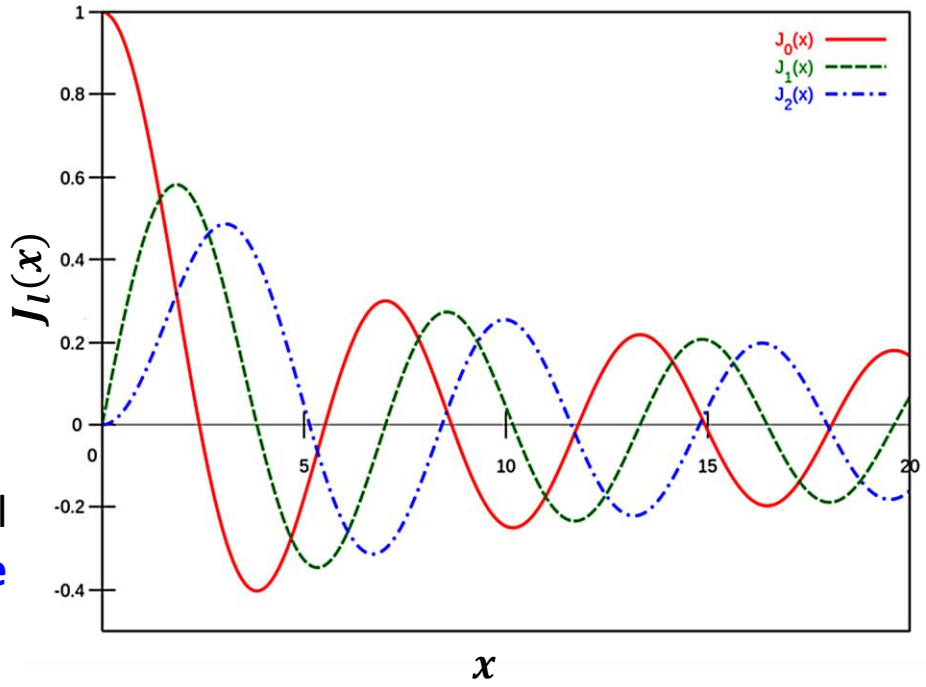

Therefore, the zeros of the Bessel function are labeled by two indices and are denoted by $\alpha_{n,l}$.

5.3 QUANTUM WIRE

5.3.3 GaAs Nanowire : Subbands and probability density

$$\Psi(\vec{r}) = aJ_l\left(\sqrt{\frac{2m^*\mathcal{E}}{\hbar^2}}\rho\right)\left(\mathrm{A}e^{il\theta} + \mathrm{B}e^{-il\theta}\right)e^{ik_z z}$$

$$\mathcal{E} = E - \frac{\hbar^2 k_z^2}{2m^*}$$

Imposing the boundary condition $u(R) = 0$ is equivalent to requiring:

$$J_l\left(\sqrt{\frac{2m^*\mathcal{E}}{\hbar^2}}R\right) = 0 \quad \text{that is} \quad \sqrt{\frac{2m^*\mathcal{E}}{\hbar^2}}R = \alpha_{n,l}$$

We then obtain the **energy levels**:

$$E = \frac{\hbar^2\alpha_{n,l}^2}{2m^*R^2} + \frac{\hbar^2 k_z^2}{2m^*}$$

This expression defines the **subbands**, i.e., parabolic dispersion relations in k_z, each shifted upward by $\frac{\hbar^2\alpha_{n,l}^2}{2m^*R^2}$.

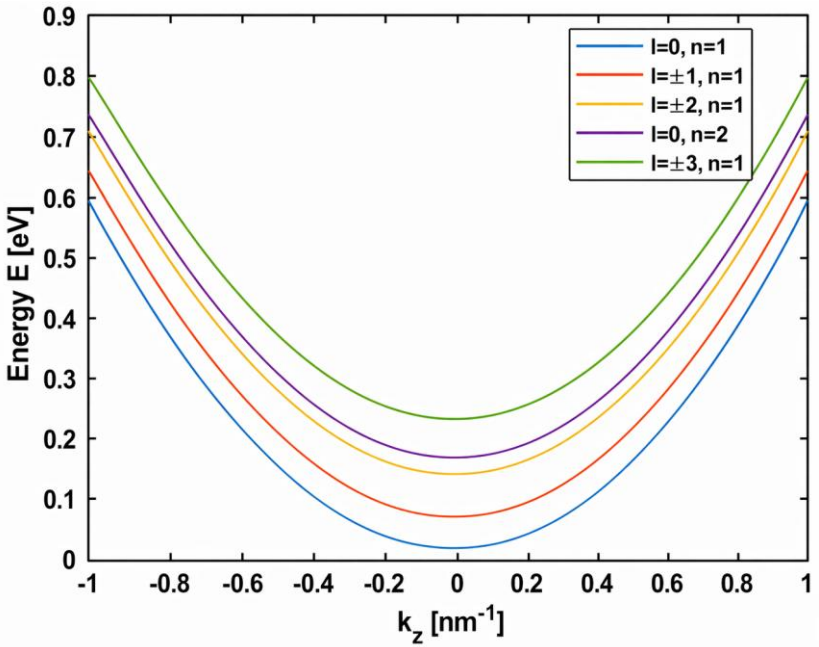

Figure 2: Energies E of the five lowest subbands as a function of k_z for a GaAs nanowire with radius $R = 10$ nm.

5.3 QUANTUM WIRE

5.3.3 GaAs Nanowire : Subbands and probability density

$$\Psi(\vec{r}) = aJ_l\left(\sqrt{\frac{2m^*\mathcal{E}}{\hbar^2}}\rho\right)\left(\mathrm{A}e^{il\theta} + \mathrm{B}e^{-il\theta}\right)e^{ik_z z}$$

The **probability density** is defined as the square modulus of the wave function.

Since the angular and longitudinal parts have unit modulus, the probability density depends only on the radial contribution:

$$|\Psi(\vec{r})|^2 = a^2 J_l\left(\sqrt{\frac{2m^*\mathcal{E}}{\hbar^2}}\rho\right)^2$$

Normalizing over the radial coordinate from the center of the wire to $\rho = R$, the constant a is determined by:

$$a^2 = \frac{1}{\int_0^R J_l\left(\sqrt{\frac{2m^*\mathcal{E}}{\hbar^2}}\rho\right)^2 d\rho}$$

Just as the subband energies depend on the two quantum numbers n and l, the probability density also depends on them.

5.3 QUANTUM WIRE

5.3.3 GaAs Nanowire : Subbands and probability density

To analyze this dependence, we first fix one quantum number and then vary the other, for a GaAs nanowire with $R = 10\ \mathrm{nm}$.

Let us fix $\mathbf{n = 1}$ (the lowest value). The probability densities for the 4 lowest values of l are shown in Figure.

For $l = 0$, the electron is mainly localized at the center of nanowire, with no probability of being found at surface.

As l increases, the probability peak shifts toward the surface, where the electron is more likely to be found.

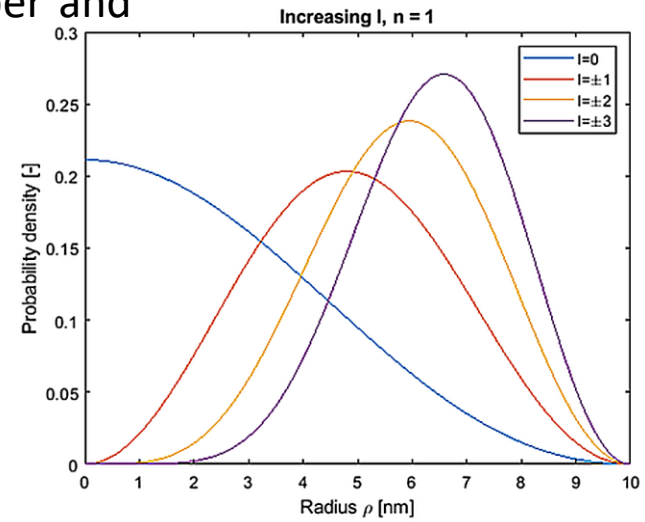

We set the angular momentum to $\mathbf{l = 0}$ (the lowest value). The probability densities for the 4 lowest values of n are shown in Figure.

As n increases, a new radial node is introduced, so the number of nodes is $n - 1$.

A larger number of nodes corresponds to shorter wavelengths and, consequently, higher energies.

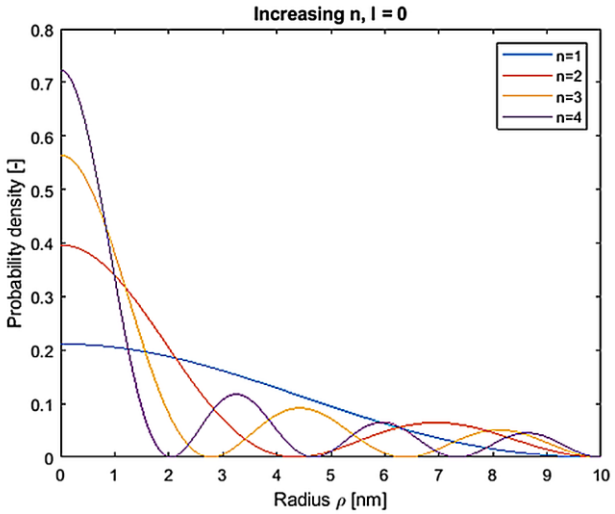

5.4 QUANTUM DOT

5.4.1 Density of states

An **ideal quantum dot** is a structure that confines electrons in all three spatial dimensions. As a result, no quasi-free motion is possible in any direction, and the energy spectrum is fully discrete, similarly to that of an atom.

For a quantum dot with a rectangular parallelepiped geometry growth on a substrate, the electron wave function has no plane-wave component, and the energy can be expressed as the sum of three discrete contributions:

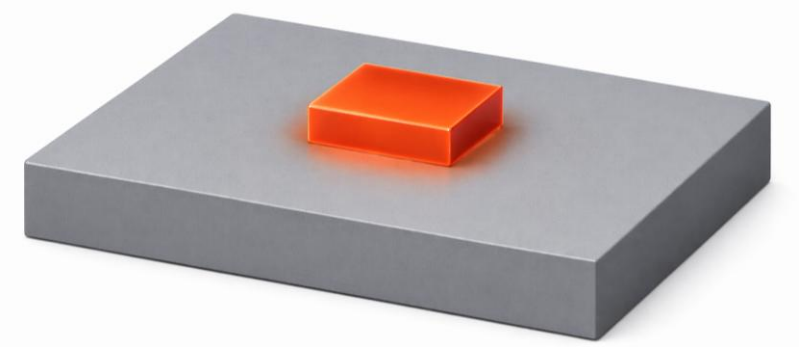

$$E(n,m,l) = (\mathrm{E}_x)_n + \left(\mathrm{E}_y\right)_m + (\mathrm{E}_z)_l = \frac{\hbar^2 (k_x^2)_n}{2m^*} + \frac{\hbar^2 \left(k_y^2\right)_m}{2m^*} + \frac{\hbar^2 (k_z^2)_l}{2m^*}$$

where n, m, and l are integers that label the quantized energy levels $(E_x)_n$, $\left(E_y\right)_m$, and $(E_z)_l$, as well as the corresponding quantized wavevectors $(k_x)_n$, $\left(k_y\right)_m$, and $(k_z)_l$, arising from the confinement along the x, y, and z directions.

The values of $(E_x)_n$, $\left(E_y\right)_m$, and $(E_z)_l$ can be determined more accurately by solving the finite potential well problem.

5.4 QUANTUM DOT

5.4.1 Density of states

The density of states of electrons in the conduction band is given by:

$$g_{1D}(E) = 2\sum_{n,m,l} \delta\left[(\mathrm{E}_x)_n + (\mathrm{E}_y)_m + (\mathrm{E}_z)_l - E\right]$$

The density of states is therefore a sum of Dirac delta functions, corresponding to the discrete energy levels $E(n, m, l)$.

Because quantum dots have a fully discrete, atom-like energy spectrum, they can be visualized and described as "**artificial atoms**."

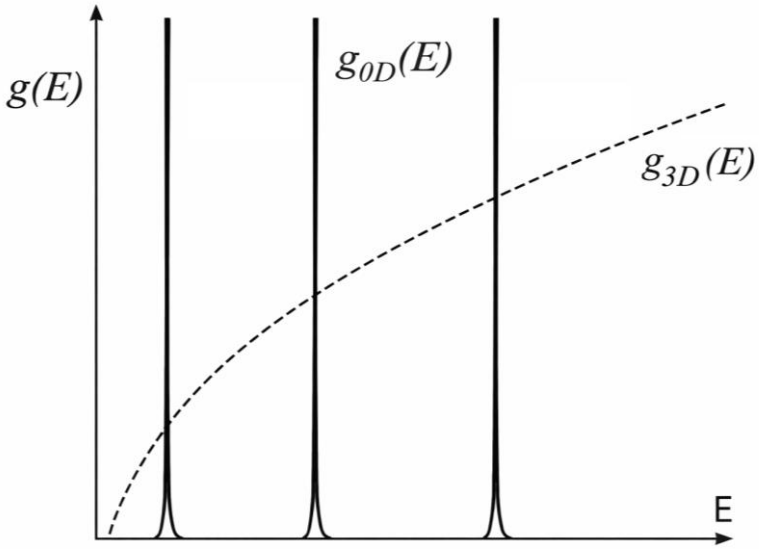

This discretization leads to carrier dynamics that are markedly different from those in higher-dimensional systems, where the density of states is continuous over a range of energies.

Therefore, since only specific energy levels are allowed, changes in the electronic configuration are more restricted.

5.4 QUANTUM DOT

5.4.2 Energy levels in a spherical potential well

A quantum dot can be modeled as a **spherically symmetric confinement region**, where the electron experiences a centrosymmetric potential depending only on the radial distance r.

The starting point for the problem of a particle in a centrosymmetric potential is the Schrödinger equation:

$$-\frac{\hbar^2}{2m}\nabla^2\psi(\vec{r}) + V(\vec{r})\psi(\vec{r}) = E\psi(\vec{r})$$

Let us assume that the potential is zero inside the quantum dot and infinite outside, as in the nanowire case. Then:

$$-\frac{\hbar^2}{2m}\nabla^2\psi(\vec{r}) = E\psi(\vec{r})$$

Given the spherical symmetry of the problem, it is convenient to introduce spherical coordinates. The relations between Cartesian and spherical coordinates are:

$$\begin{cases} x = rsen\theta cos\phi \\ y = rsen\theta sen\phi \\ z = rcos\theta \end{cases}$$

5.4 QUANTUM DOT

5.4.2 Energy levels in a spherical potential well

$$-\frac{\hbar^2}{2m}\nabla^2\psi(\vec{r}) = E\psi(\vec{r})$$

We can express the Laplacian operator in spherical coordinates as:

$$\nabla^2 = \frac{1}{r^2}\frac{\partial}{\partial r}r^2\frac{\partial}{\partial r} + \frac{1}{r^2 sen\theta}\frac{\partial}{\partial\theta}\left(sen\theta\frac{\partial}{\partial\theta}\right) + \frac{1}{r^2 sen^2\theta}\frac{\partial^2}{\partial\phi^2}$$

Introducing the angular momentum operator:

$$\Lambda^2 = \frac{1}{sen\theta}\frac{\partial}{\partial\theta}\left(sen\theta\frac{\partial}{\partial\theta}\right) + \frac{1}{sen^2\theta}\frac{\partial^2}{\partial\phi^2}$$

we can write the Laplacian operator as:

$$\nabla^2 = \frac{1}{r^2}\frac{\partial}{\partial r}r^2\frac{\partial}{\partial r} + \frac{1}{r^2}\Lambda^2$$

In this form, the operator Λ^2 accounts for the angular part of the Hamiltonian, while the remaining term describes the radial contribution.

5.4 QUANTUM DOT

5.4.2 Energy levels in a spherical potential well

$$-\frac{\hbar^2}{2m}\nabla^2\psi(\vec{r}) = E\psi(\vec{r})$$

$$\nabla^2 = \frac{1}{r^2}\frac{\partial}{\partial r}r^2\frac{\partial}{\partial r} + \frac{1}{r^2}\Lambda^2$$

Substituting into the Schrödinger equation and assuming separation of variables into a radial part $R(r)$ and an angular part $\Upsilon(\theta,\varphi)$, we write:

$$\psi(\vec{r}) = R(r)\Upsilon(\theta,\varphi)$$

This leads to:

$$\frac{\partial}{\partial r}r^2\frac{\partial[R(r)\Upsilon(\theta,\varphi)]}{\partial r} + \Lambda^2[R(r)\Upsilon(\theta,\varphi)] = -\frac{2mr^2E}{\hbar^2}R(r)\Upsilon(\theta,\varphi)$$

Dividing both sides by $R(r)\Upsilon(\theta,\varphi)$, we obtain:

$$\frac{1}{R(r)}\frac{\partial}{\partial r}r^2\frac{\partial R(r)}{\partial r} + \frac{1}{\Upsilon(\theta,\varphi)}\Lambda^2\Upsilon(\theta,\varphi) = -\frac{2mr^2E}{\hbar^2}$$

Thus, for a given value of r, the angular dependence can be determined by solving the angular part of the Schrödinger equation.

5.4 QUANTUM DOT

5.4.2 Energy levels in a spherical potential well

$$\frac{1}{R(r)}\frac{\partial}{\partial r}r^2\frac{\partial R(r)}{\partial r}+\frac{1}{\Upsilon(\theta,\varphi)}\Lambda^2\Upsilon(\theta,\varphi)=-\frac{2mr^2E}{\hbar^2}$$

$$\Lambda^2\Upsilon(\theta,\varphi)=\mathcal{E}\Upsilon(\theta,\varphi)$$

where $\mathcal{E}$ are the eigenvalues associated with the angular part.

This is the eigenvalue equation for the angular momentum operator in spherical coordinates, and its eigenfunctions are:

$$\mathcal{E}\Upsilon(\theta,\varphi)=Ae^{im_l\varphi}P_l(cos\theta)$$

where $P_l(cos\theta)$ are Legendre polynomials and m is an integer.

For a given l, the quantum number m takes the values $m=-l,-l+1,\dots,l$ and the corresponding eigenvalues are:

$$\mathcal{E}=-l(l+1)$$

Substituting into the Schrödinger equation, we obtain the radial equation:

$$\frac{1}{R(r)}\frac{\partial}{\partial r}r^2\frac{\partial R(r)}{\partial r}-l(l+1)=-\frac{2mEr^2}{\hbar^2}$$

5.4 QUANTUM DOT

5.4.2 Energy levels in a spherical potential well

$$\frac{1}{R(r)}\frac{\partial}{\partial r}r^2\frac{\partial R(r)}{\partial r} - l(l-1) = -\frac{2mEr^2}{\hbar^2}$$

Let us introduce $u(r) = rR(r)$

and substitute it into the radial equation:

$$\frac{r}{u(r)}\frac{\partial}{\partial r}r^2\frac{\partial}{\partial r}\left[\frac{u(r)}{r}\right] - l(l-1) = -\frac{2mEr^2}{\hbar^2}$$

Let us evaluate the first derivative:

$$\frac{\partial}{\partial r}\left[\frac{u(r)}{r}\right] = \frac{u'(r)r - u(r)}{r^2}$$

Therefore: $\frac{\partial}{\partial r}r^2\frac{\partial}{\partial r}\left[\frac{u(r)}{r}\right] = \frac{\partial}{\partial r}[u'(r)r - u(r)] = u''(r)r + u'(r) - u'(r) = u''(r)r$

Substituting, we obtain:

$$\frac{r^2}{u(r)}\frac{\partial^2 u(r)}{\partial r^2} - l(l+1) = -\frac{2mEr^2}{\hbar^2}$$

5.4 QUANTUM DOT

5.4.2 Energy levels in a spherical potential well

$$\frac{r^2}{u(r)}\frac{\partial^2 u(r)}{\partial r^2} - l(l+1) = -\frac{2mEr^2}{\hbar^2}$$

that is :

$$\frac{\partial^2 u(r)}{\partial r^2} = \left[\frac{l(l+1)}{r^2} - \frac{2mE}{\hbar^2}\right] u(r)$$

Introducing $k^2 = \frac{2mE}{\hbar^2}$, we can rewrite the equation as:

$$\frac{\partial^2 u(r)}{\partial r^2} = \left[\frac{l(l+1)}{r^2} - k^2\right] u(r)$$

Far from the origin, where the term $\frac{l(l+1)}{r^2}$ becomes negligible, the equation reduces to:

$$\frac{d^2 u(r)}{dr^2} \approx -k^2 u(r)$$

whose solutions are sinusoidal functions:

$$u(r) \sim \sin(kr), \cos(kr).$$

5.4 QUANTUM DOT

5.4.2 Energy levels in a spherical potential well

$$\frac{\partial^2 u(r)}{\partial r^2} = \left[\frac{l(l+1)}{r^2} - k^2\right] u(r)$$

Near the origin, the solutions are spherical Bessel functions:

$$u_l(r) = \alpha r j_l(kr)$$

$$j_l(x) = (-x)^l \left(\frac{1}{x}\frac{d}{dx}\right)^l \frac{senx}{x}$$

We obtain one eigenfunction for each value of l.

The lowest level corresponds to $l = 0$ for which:

$$u_0(r) = \alpha r j_0(kr) = \alpha r \frac{sen(kr)}{kr}$$

and therefore:

$$R_0(r) = \frac{u_0(r)}{r} = \alpha \frac{sen(kr)}{kr}$$

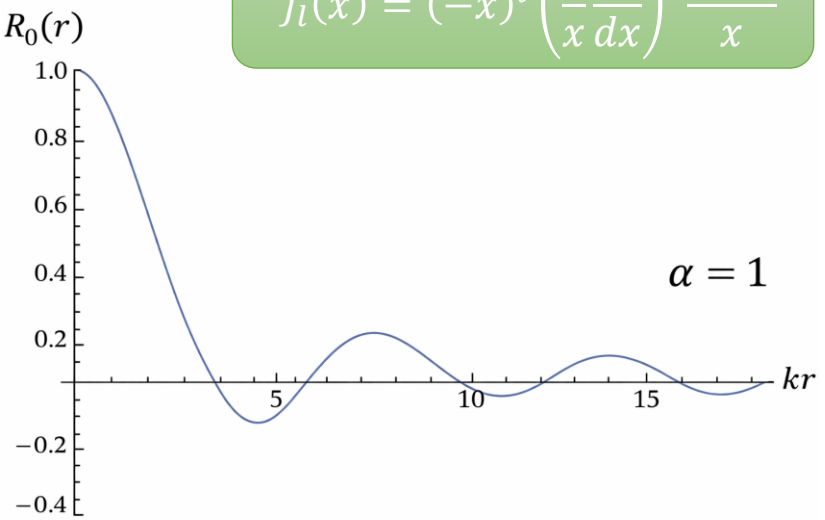

Since these functions possess a countably infinite number of zeros—similarly to the cylindrical harmonics in quantum wires—the index n labels the different energy levels according to the boundary condition that the wavefunction vanishes at the surface of the quantum dot.

5.4 QUANTUM DOT

5.4.3 Thermal and non-thermal distribution of the population

The energy levels discussed so far were obtained by assuming an ideal spherical potential, equal to zero inside the quantum dot and infinite outside.

In a more realistic scenario, one must consider a finite potential inside the quantum dot and a higher potential outside. In this sense, a quantum dot can be modeled as a spherical quantum well. The calculations follow the same steps as before, with the additional complexity of including a finite confining potential in the Schrödinger equation.

The energy levels remain discrete; however, their values (and spacing) depend on geometrical parameters such as the size of the dot and the depth of the potential.

Let us now consider **a spatial distribution of quantum dots** on a substrate.

In realistic systems, quantum dots are typically arranged in ensembles rather than isolated structures, forming arrays with a certain degree of size and position dispersion.

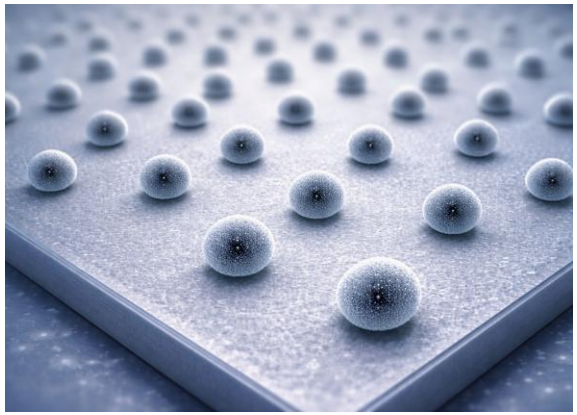

This distribution plays a crucial role in determining the overall optical and electronic properties of the system and influences the collective behavior of carriers.

5.4 QUANTUM DOT

5.4.3 Thermal and non-thermal distribution of the population

The Figure represents the band diagram of a **quantum dot embedded in a semiconductor matrix**, with the confined electron (E_e) and hole (E_h) energy levels within the potential well.

It illustrates carrier **capture into the dot** from the surrounding material and **escape processes back to the continuum**, as well as **radiative recombination**, indicated by the emitted photon energy $\hbar\omega = E_g + E_e + E_h$.

We define the localization energy E_{loc} as the energy difference between the confined level and the top of the potential barrier.

Carriers can escape from the quantum dot by overcoming the barrier and leaving the confinement region.

This process becomes more significant as the temperature increases and the effective localization energy decreases.

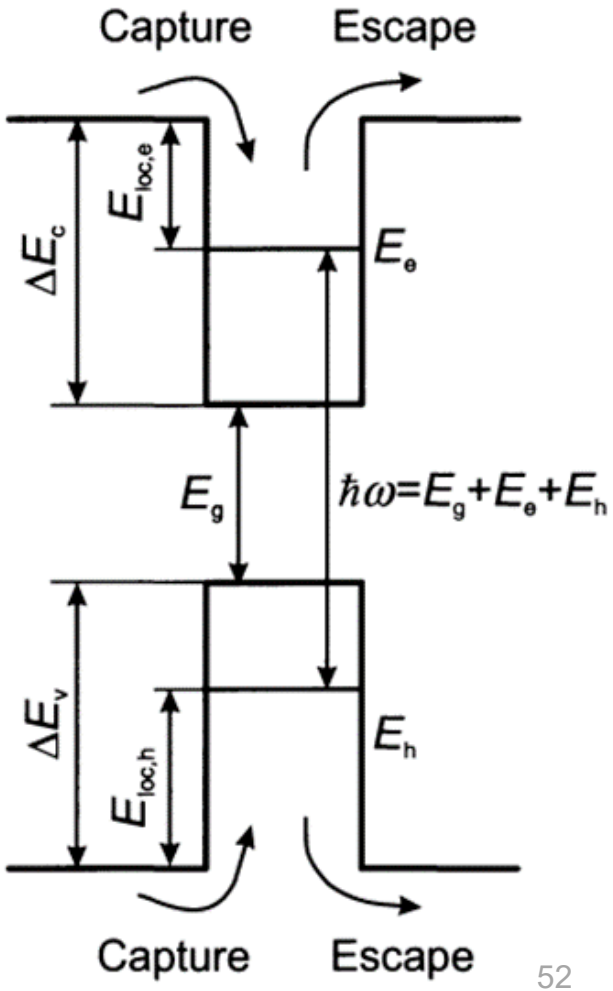

5.4 QUANTUM DOT

5.4.3 Thermal and non-thermal distribution of the population

Alternatively, an electron may recombine with an available hole state.

Under steady-state conditions, the **average electron–hole recombination rate** in a quantum dot must equal **the net capture rate**, defined as the difference between the carrier capture rate and the escape rate from the dot.

Let us define:

f_n and f_p as the occupation probabilities for electrons ar holes in the bound states of the quantum dot.

n and p as the carrier densities in the barrier, i.e., in th surrounding material (substrate).

n_1 and p_1 as the escape rates for electrons and holes from the quantum dot to the barrier due to thermal effects.

ν_n and ν_p as the capture rates for electrons and holes into the quantum dot from the barrier.

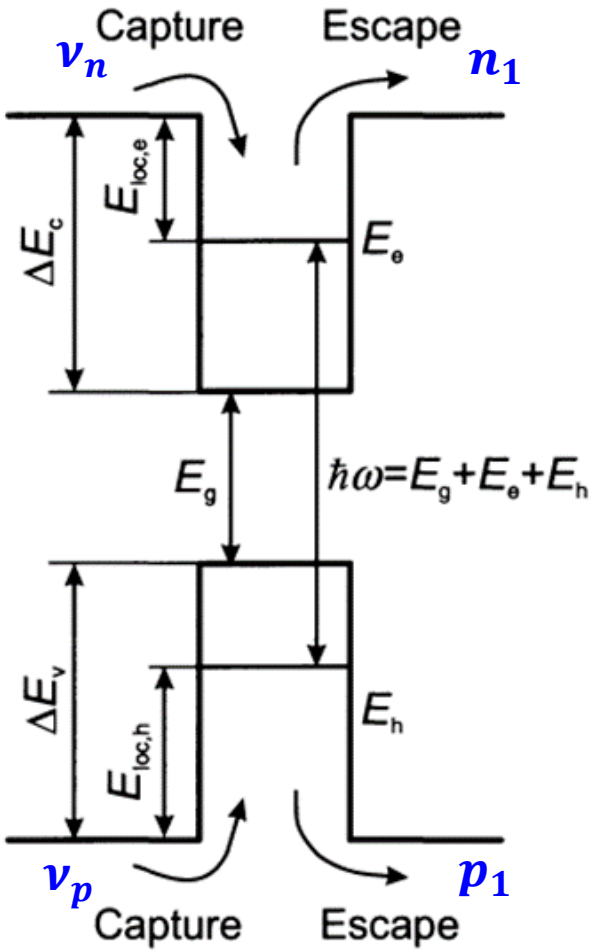

5.4 QUANTUM DOT

5.4.3 Thermal and non-thermal distribution of the population

Averaging over all quantum dots (denoted by $\langle\cdot\rangle$), the net capture rate can be written as:

$$v_n n(1-\langle f_n\rangle) - n_1\langle f_n\rangle = v_p p\big(1-\langle f_p\rangle\big) - n_1\langle f_p\rangle$$

The average electron–hole recombination rate can be expressed as the product of the occupation probabilities divided by a characteristic **recombination time** τ_D, $\frac{\langle f_n f_p\rangle}{\tau_D}$.

Under steady-state conditions, we obtain:

$$\frac{\langle f_n f_p\rangle}{\tau_D} = v_n n(1-\langle f_n\rangle) - n_1\langle f_n\rangle = v_p p\big(1-\langle f_p\rangle\big) - p_1\langle f_p\rangle$$

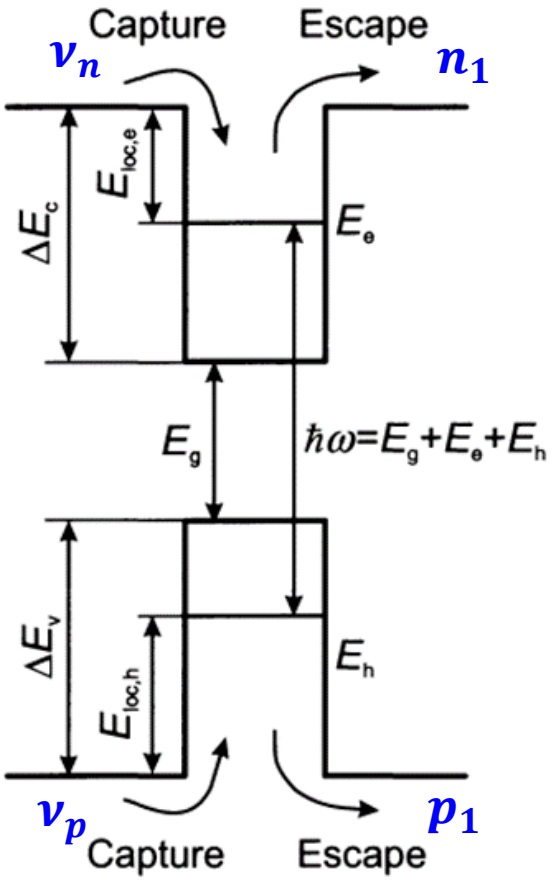

We can identify two distinct limiting cases:

If the recombination of carriers inside the quantum dot is much faster than the escape rate, the population becomes independent of the carrier energy. As a result, quantum dots of different sizes exhibit the same population.

Dots behave as **non-interacting systems**, with no exchange of carriers.

5.4 QUANTUM DOT

5.4.3 Thermal and non-thermal distribution of the population

$$\frac{\langle f_n f_p \rangle}{\tau_D} = v_n n(1 - \langle f_n \rangle) - n_1 \langle f_n \rangle = v_p p\big(1 - \langle f_p \rangle\big) - p_1 \langle f_p \rangle$$

In the opposite case, when carriers can escape from the quantum dot several times before recombining (with a probability that depends on the localization energy), thermal equilibrium is established between the barrier and the quantum dot.

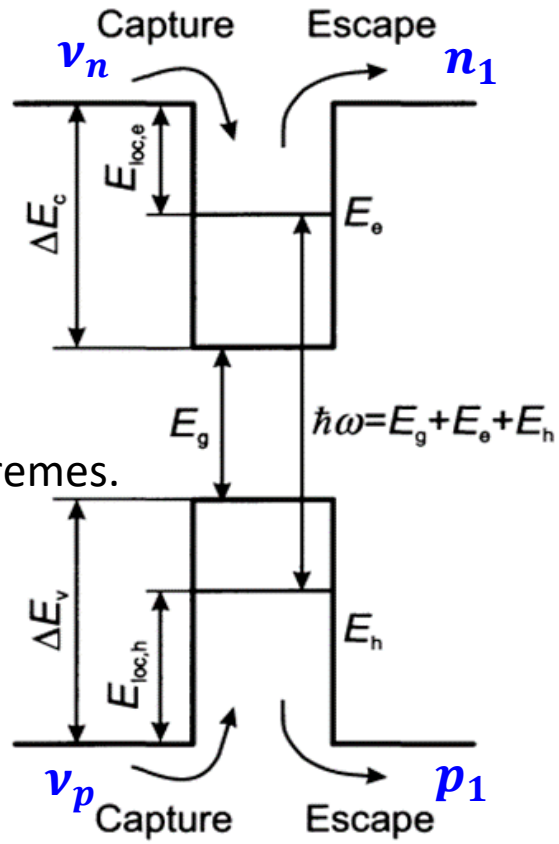

In real systems, the situation typically lies between these two extremes.

At thermal equilibrium, the **escape time** τ_e from a trap (neglecting other loss mechanisms) is empirically given by:

$$\tau_e, \tau_p \approx \tau_o e^{\frac{E_{loc}}{KT}}$$

with $\tau_o \approx 10\ ps$, corresponding to $E_{loc} = 0$.

At room temperature, the escape time is approximately $\tau_e \approx 1$ ns, which is comparable to the typical radiative recombination time. Therefore, **τ_e and τ_D are of the same order of magnitude**.

5.4 QUANTUM DOT

5.4.3 Thermal and non-thermal distribution of the population

$$\frac{\langle f_n f_p \rangle}{\tau_D} = v_n n(1 - \langle f_n \rangle) - n_1 \langle f_n \rangle = v_p p\big(1 - \langle f_p \rangle\big) - p_1 \langle f_p \rangle$$

Let's analyze the two extreme cases:

If the **characteristic escape time is much shorter than the radiative recombination time**, i.e., $\tau_e, \tau_p \ll \tau_D$, carriers can redistribute among the different quantum dots, and a thermal distribution is established.

In this regime, the population is described by Fermi–Dirac distribution functions with quasi-Fermi levels E_{F_c} and E_{F_v}:

$$f_n\big(E_e, E_{F_c}\big) = \frac{1}{1 + e^{\frac{E_e - E_{F_c}}{KT}}} \qquad f_p\big(E_e, E_{F_v}\big) = \frac{1}{1 + e^{\frac{E_h - E_{F_v}}{KT}}}$$

Under these conditions, the net recombination rate can be set to zero, and therefore:

$$v_n n(1 - \langle f_n \rangle) - n_1 \langle f_n \rangle = v_p p\big(1 - \langle f_p \rangle\big) - p_1 \langle f_p \rangle = 0$$

5.4 QUANTUM DOT

5.4.3 Thermal and non-thermal distribution of the population

$v_n n(1-\langle f_n\rangle) - n_1\langle f_n\rangle = 0$

$v_p p(1-\langle f_p\rangle) - p_1\langle f_p\rangle = 0$

v_n capture rates
n_1 escape rates

From these relations, we can obtain the densities of free carriers:

$$\frac{n}{n_1} = \frac{\langle f_n\rangle}{v_n(1-\langle f_n\rangle)} \qquad \frac{p}{p_1} = \frac{\langle f_p\rangle}{v_p(1-\langle f_p\rangle)}$$

The electron density in the substrate, if the quasi-Fermi level E_{F_c} lies several kT below the barrier, is given by:

$$n = N_c e^{\frac{E_{F_c} - \Delta E_c}{KT}}$$

with $N_c = 2\left(\frac{mKT}{2\pi\hbar^2}\right)^{3/2}$

A similar expression holds for holes.

$$f_p(E_e, E_{F_v}) = \frac{1}{1 + e^{\frac{E_h - E_{F_v}}{KT}}}$$

$$f_n(E_e, E_{F_c}) = \frac{1}{1 + e^{\frac{E_e - E_{F_c}}{KT}}}$$

By substituting n and f_n, the ratio between escape and capture rates can be expressed as a function of temperature.

5.4 QUANTUM DOT

5.4.3 Thermal and non-thermal distribution of the population

$$\frac{\langle f_n f_p \rangle}{\tau_D} = v_n n(1 - \langle f_n \rangle) - n_1 \langle f_n \rangle = v_p p\big(1 - \langle f_p \rangle\big) - p_1 \langle f_p \rangle$$

v_n capture rates
n_1 escape rates

The other limiting case corresponds to radiative recombination being much faster than the thermal escape of carriers from the quantum dot, i.e. $\tau_e, \tau_p \gg \tau_D$.

In this case, starting from the steady-state equation, we can neglect n_1 and p_1, so that the carrier density in the barrier becomes:

$$n = \frac{\langle f_n f_p \rangle}{\tau_D} \frac{1}{v_n} \frac{1}{(1 - \langle f_n \rangle)}$$

where f_n and f_p represent non-equilibrium populations.

Intermediate situations are more difficult to analyze. One must also take into account that electrons and holes may have different localization energies. A further complication arises when **excited states** are included, since they can act as intermediate levels for the capture or escape of electrons and holes.

5.4 QUANTUM DOT

5.4.4 Carrier Statistics: Rate Equations and Random Population

The conventional **rate-equation method** describes the population of the i-th (non-degenerate) electron level in terms of the average occupation probability f_i. However, when multiple levels are involved, a more detailed approach is required.

For a set of N_D quantum dots, we introduce the variable γ_i^j, which indicates whether the i-th electronic level in the j-th dot is occupied ($\gamma_i^j = 1$) or empty ($\gamma_i^j = 0$).

The average occupation of the i-th level is then:

$$f_i = \frac{1}{N_D}\sum_{j=1}^{N_D}\gamma_i^j$$

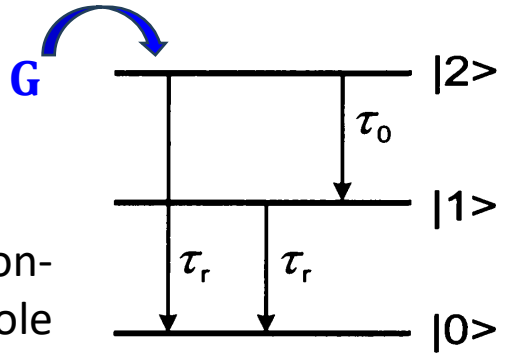

Within the rate-equation framework, we consider two non-degenerate energy levels associated with electron–hole pairs (formed by an electron and a hole in states with the same quantum numbers).

We denote by f_1 and f_2 the populations of these two levels, with $0 \le f_i \le 1$.

Let us assume a generation (excitation) rate G that populates the upper level.

5.4 QUANTUM DOT

5.4.4 Carrier Statistics: Rate Equations and Random Population

We assume the same mean lifetime τ_r for both levels toward the ground state $|0\rangle$ and denote by τ_0 the intrinsic relaxation time from level $|2\rangle$ to level $|1\rangle$, as shown in the Figure.

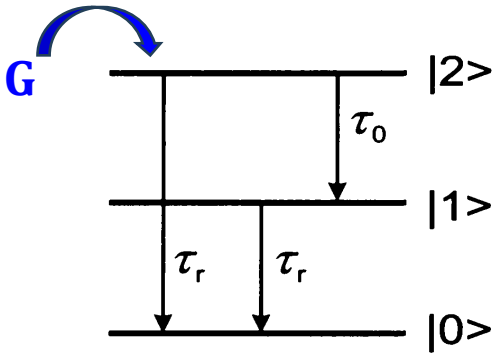

The rate equations for level $|2\rangle$ and level $|1\rangle$ are:

$$\frac{df_2}{dt} = -\frac{f_2}{\tau_r} - \frac{f_2(1-f_1)}{\tau_0} + G$$

$$\frac{df_1}{dt} = -\frac{f_1}{\tau_r} + \frac{f_2(1-f_1)}{\tau_0}$$

The ground state $|0\rangle$ is not explicitly included in the dynamics, since carriers relaxing to this level rapidly recombine radiatively and leave the system.

An analytical solution can be obtained in the **steady-state** regime.

By imposing: $\frac{df_1}{dt} + \frac{df_2}{dt} = 0$

We obtain:

$$-\frac{f_2}{\tau_R} - \frac{f_2(1-f_1)}{\tau_0} + G - \frac{f_1}{\tau_r} + \frac{f_2(1-f_1)}{\tau_0} = 0$$

5.4 QUANTUM DOT

5.4.4 Carrier Statistics: Rate Equations and Random Population

$$-\frac{f_2}{\tau_r}-\frac{f_2(1-f_1)}{\tau_0}+G-\frac{f_1}{\tau_r}+\frac{f_2(1-f_1)}{\tau_0}=0$$

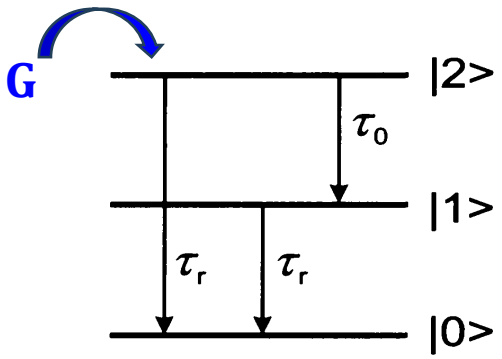

which simplifies to:

$$-\frac{f_2}{\tau_r}+G=\frac{f_1}{\tau_r}$$

If the generation rate is low $\left(G \ll \frac{1}{\tau_r}\right)$, we can assume $f_2 \approx 0$, and therefore:

$$f_1 = G\tau_r$$

Thus, $f_1 N_D$ quantum dots are occupied by one electron–hole pair, while the remaining dots are empty.

If an electron–hole pair is captured by the quantum dot ensemble, two situations may occur:

if it is captured by an **empty quantum dot**, f_2 remains zero;

if it is captured by one of the $\mathbf{f_1 N_D}$ **quantum dots** already occupied by an electron–hole pair, then $f_2 > 0$, contradicting the assumption $f_2 \approx 0$.

5.4 QUANTUM DOT

5.4.4 Carrier Statistics: Rate Equations and Random Population

$$-\frac{f_2}{\tau_r}-\frac{f_2(1-f_1)}{\tau_0}+G-\frac{f_1}{\tau_r}+\frac{f_2(1-f_1)}{\tau_0}=0$$

$$f_1 = G\tau_r$$
$$f_2 \approx 0$$

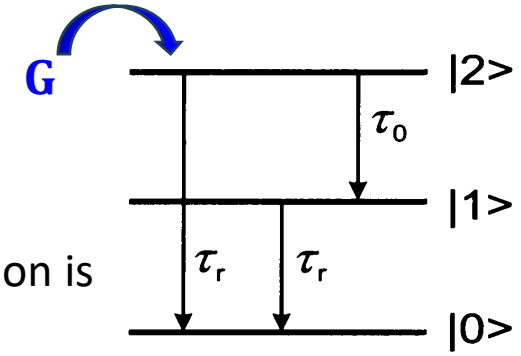

In summary:

If the generation rate is low, the probability of double occupation is negligible, and we can assume:

$$f_2 \approx 0$$

In this regime, each quantum dot can host at most one electron–hole pair.

However, carrier capture is a stochastic process, and in principle a new electron–hole pair can also be captured by an already occupied quantum dot.

In this case, a doubly occupied state would be formed, implying:

$$f_2 > 0$$

This leads to an inconsistency, since the assumption $f_2 \approx 0$ neglects these events.

Therefore, the rate-equation model is only valid as an approximate description in the low excitation regime.

5.4 QUANTUM DOT

5.4.4 Carrier Statistics: Rate Equations and Random Population

An alternative to the rate-equation model is to describe the system in terms of **master equations** for the microstates of a set of quantum dots.

The ensemble is characterized by the number N_k of quantum dots in each configuration k, defined by a specific set of occupation variables γ_i^j.

The total number of quantum dots is conserved, and therefore:

$$\sum_k N_k = N_D$$

When a capture or recombination event occurs, a quantum dot transitions from one configuration k_1 to another configuration k_2. At the ensemble level, this corresponds to a change $N_{k_1} \rightarrow N_{k_1} - 1$and $N_{k_2} \rightarrow N_{k_2} + 1$.

The identity of the specific quantum dot undergoing the transition is irrelevant. Therefore, the system can be described statistically using the **random population approximation**, in which we write differential equations for the time evolution of N_k. This approach is valid in the limit of a large number of quantum dots N_D.

5.4 QUANTUM DOT

5.4.4 Carrier Statistics: Rate Equations and Random Population

A consistent description of the two-level system is then obtained by considering all possible microstates and their transitions, as illustrated in the Figure.

We describe the quantum dots in terms of double-index states, where each index refers to the occupation of one of the two energy levels, $|2\rangle$ or $|1\rangle$. Thus:

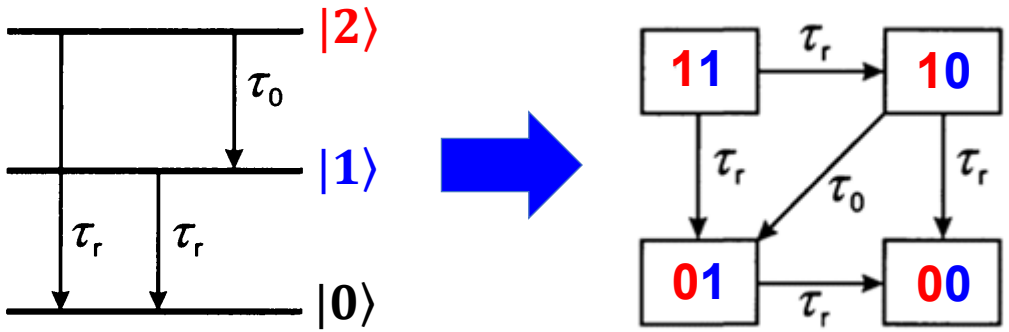

(0,0) denotes a quantum dot with both level $|2\rangle$ empty and $|1\rangle$ empty

(1,0) a quantum dot with $|2\rangle$ occupied and $|1\rangle$ empty,

(0,1) a quantum dot with $|2\rangle$ empty and $|1\rangle$ occupied,

(1,1) a quantum dot with both level $|2\rangle$ and $|1\rangle$ occupied.

Let w_{00}, w_{10}, w_{01}, and w_{11} denote the probabilities of finding a quantum dot in the states (0,0), (1,0), (0,1), and (1,1), respectively.

These probabilities must satisfy the normalization condition:

$$w_{00} + w_{10} + w_{01} + w_{11} = 1$$

5.4 QUANTUM DOT

5.4.4 Carrier Statistics: Rate Equations and Random Population

The **master equations** (in the absence of external excitation) are:

$$\begin{cases} \dfrac{dw_{00}}{dt} = \dfrac{w_{10}}{\tau_r} + \dfrac{w_{01}}{\tau_r} \\ \dfrac{dw_{10}}{dt} = -\dfrac{w_{10}}{\tau_r} + \dfrac{w_{11}}{\tau_r} + \dfrac{w_{11}}{\tau_0} \\ \dfrac{dw_{01}}{dt} = -\dfrac{w_{01}}{\tau_r} + \dfrac{w_{11}}{\tau_r} - \dfrac{w_{01}}{\tau_0} \\ \dfrac{dw_{11}}{dt} = -2\dfrac{w_{11}}{\tau_R} \end{cases}$$

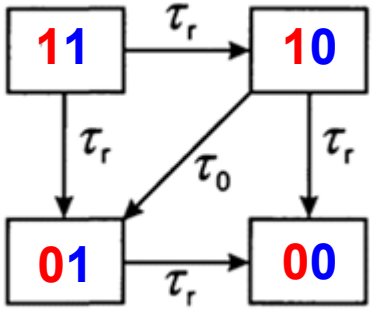

In the low-temperature limit, the probability w_n of finding a quantum dot with n carriers in level M follows a **Poisson distribution**:

$$w_n^M = \frac{\lambda^n}{n!} e^{-\lambda}$$

where $\lambda = \langle n \rangle$ is the average number of carriers in the quantum dot ensemble and depends on the external excitation level.

5.5 PHOSPHORENE AND BLACK PHOSPHORUS

5.5.1 Crystal Structure

Phosphorus is an element in group 15 of the periodic table, with atomic number 15 and chemical symbol P. It is a nonmetal belonging to the nitrogen group.

Its electronic configuration is:

$$1s^2, 2s^2, 2p^6, 3s^2, 3p^3$$

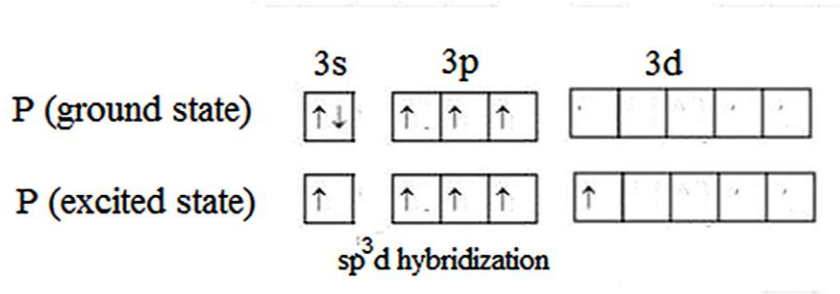

Phosphorus can promote one electron to the $3d$ orbital, resulting in five unpaired electrons and enabling sp^3d hybridization.

The electrons in the hybrid orbitals form σ bonds.

However, the promotion of an electron to the $3d$ orbital does not always occur in phosphorus compounds. In addition to compounds such as PCl_5, where sp^3d hybridization is present, there are also compounds such as PCl_3, in which phosphorus is sp^3-hybridized.

Phosphorus exists in several allotropic forms, commonly identified as **white**, **red**, and **black** phosphorus.

White phosphorus is a molecular solid composed of P_4 tetrahedra, held together by van der Waals forces.

5.5 PHOSPHORENE AND BLACK PHOSPHORUS

5.5.1 Crystal Structure

Red phosphorus is an amorphous form that does not occur naturally. It is obtained from white phosphorus by heating it to about 260°C for an extended period in the absence of air.

Black phosphorus is the most stable allotropic form.

It consists of stacked layers of individual sheets. Each sheet is composed of two **puckered double layers**.

As shown in the figure, black phosphorus is formed by a sequence of sheets stacked along the z-axis.

Adjacent sheets interact through weak van der Waals forces.

Within each sheet, atoms are arranged in two parallel sublayers (blue and red in the figure) following a well-defined pattern: zigzag chains along the y-direction alternate periodically between the upper and lower layers.

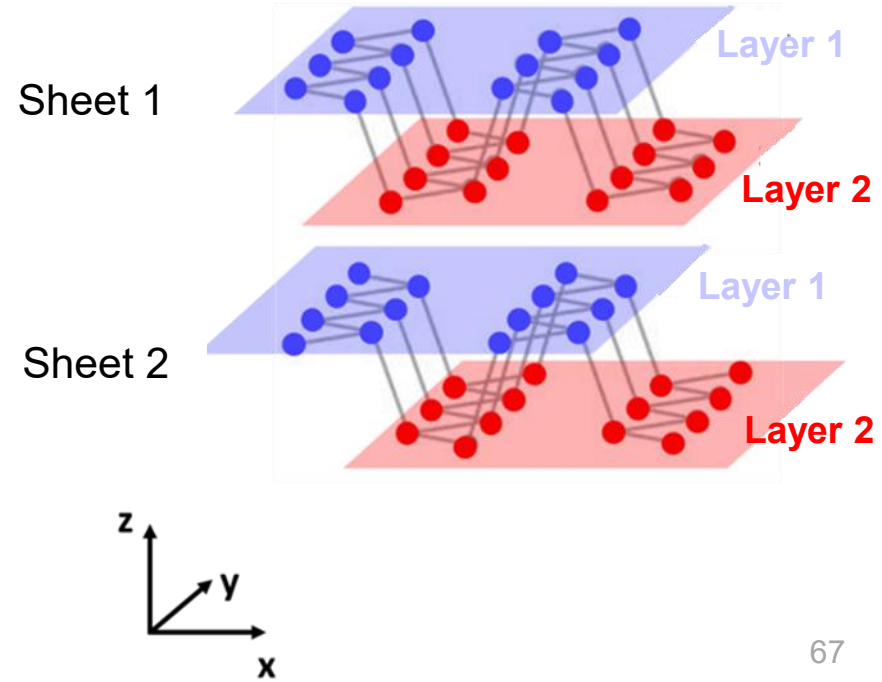

5.5 PHOSPHORENE AND BLACK PHOSPHORUS

5.5.1 Crystal Structure

It follows that, in the (zx) −plane, the atoms form a trapezoidal, wave-like periodic structure.

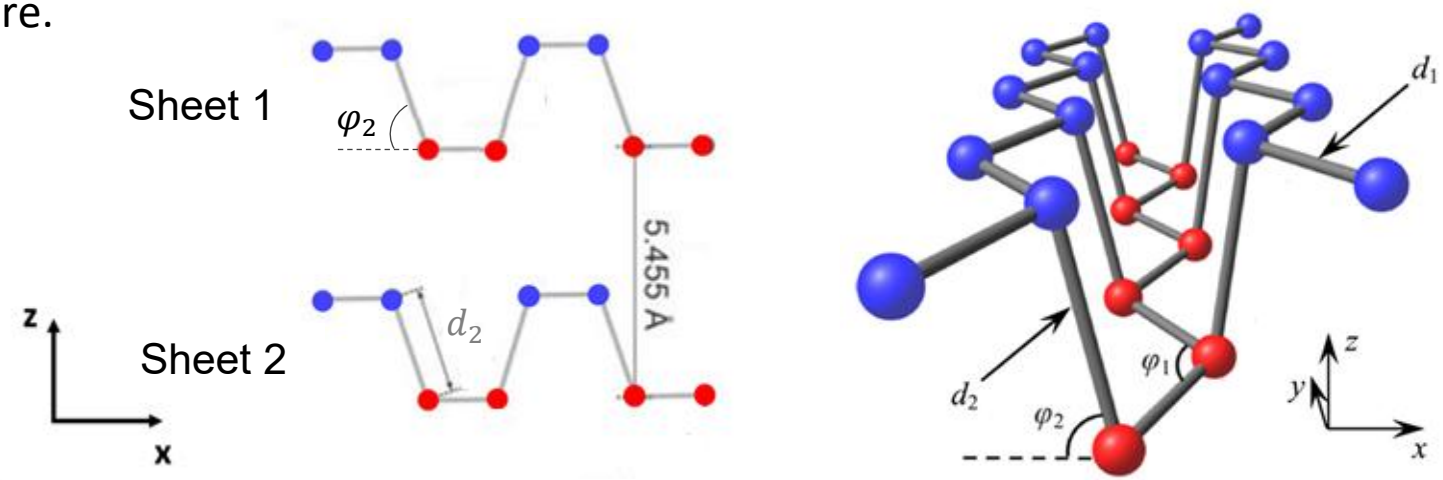

Within each sheet, each phosphorus atom (with sp^3 hybridization) is covalently bonded to three neighboring atoms.

Two of these neighbors lie in the same layer and form an angle $\varphi_1 \approx 96.34^\circ$, while the third lies in the adjacent layer and forms an angle $\varphi_2 \approx 71.1^\circ$.

The covalent bonds have slightly different lengths: the in-plane bond is $d_1 \approx 2.224$ Å, while the bond connecting atoms in different layers is $d_2 \approx 2.244$ Å

5.5 PHOSPHORENE AND BLACK PHOSPHORUS

5.5.2 Primitive cell and Brillouin zone

A single sheet of black- phosphorus is called **phosphorene**.

The main properties of black phosphorus can be derived from those of a single phosphorene layer.

Let us determine the **primitive cell** of phosphorene.

The starting point is to reduce a single sheet to a single layer.

Let us consider the projection of the structure onto the xy plane.

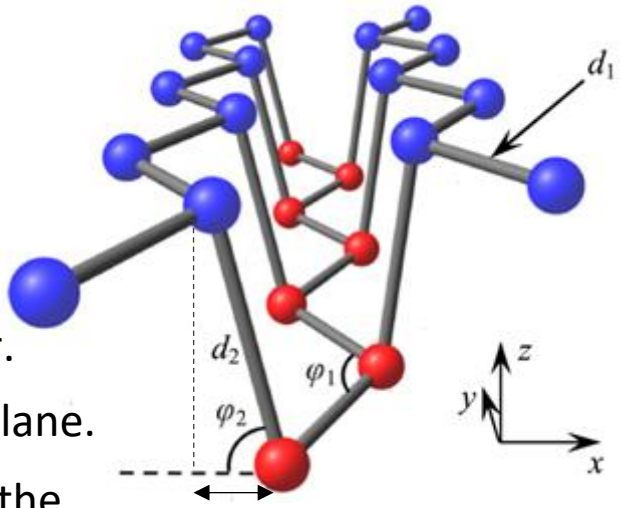

$$a = d_2 cos\varphi_2$$

Each blue atom in the upper layer, when projected onto the lower layer, has as its nearest neighbor a red atom aligned along the x-axis, at a distance:

$$a = d_2 cos\varphi_2$$

The resulting structure is a **honeycomb lattice** with irregular hexagons.

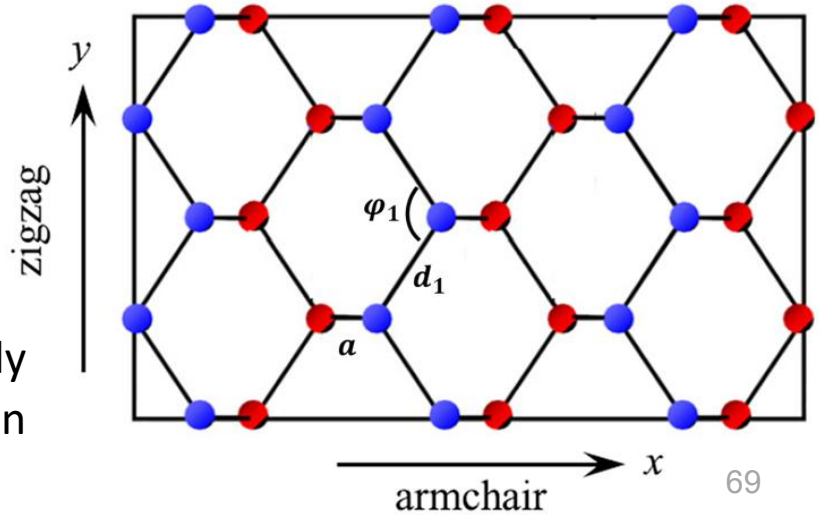

The geometry can be fully determined from the known parameters a, d_1, and φ_1.

5.5 PHOSPHORENE AND BLACK PHOSPHORUS

5.5.2 Primitive cell and Brillouin zone

Let us now determine the primitive cell by considering this two-dimensional structure.

Let us consider the center of a hexagon. From this point, we draw a vector that connects the center of the nearest neighboring hexagon along the x-direction, and the center of the nearest neighboring hexagon along the y-direction.

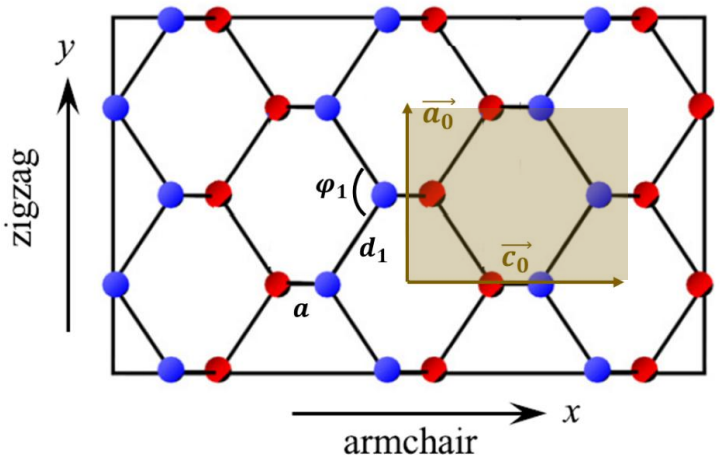

We thus identify **two lattice vectors**:

$$\overrightarrow{c_0} = c_0\widehat{u_x} \qquad \overrightarrow{a_0} = a_0\widehat{u_y}$$

It is easy to determine that $a_0 = 3.314$ Å and $c_0 = 4.376$ Å .

We note that the rectangle defined by these two orthogonal vectors constitutes a primitive cell.

This primitive cell contains **four phosphorus atoms**, since the atoms located on the edges contribute with a weight of $\frac{1}{2}$.

Its area is therefore: $A = a_0 c_0$

5.5 PHOSPHORENE AND BLACK PHOSPHORUS

5.5.2 Primitive cell and Brillouin zone

This is not the only possible choice of primitive cell.

Focusing only on the red atoms, we observe that the periodicity can be reconstructed by considering pairs of atoms located at the ends of a covalent bond d_1.

This suggests that the primitive cell can be defined by choosing two lattice vectors that connect such pairs of atoms, while preserving the symmetry of the crystal.

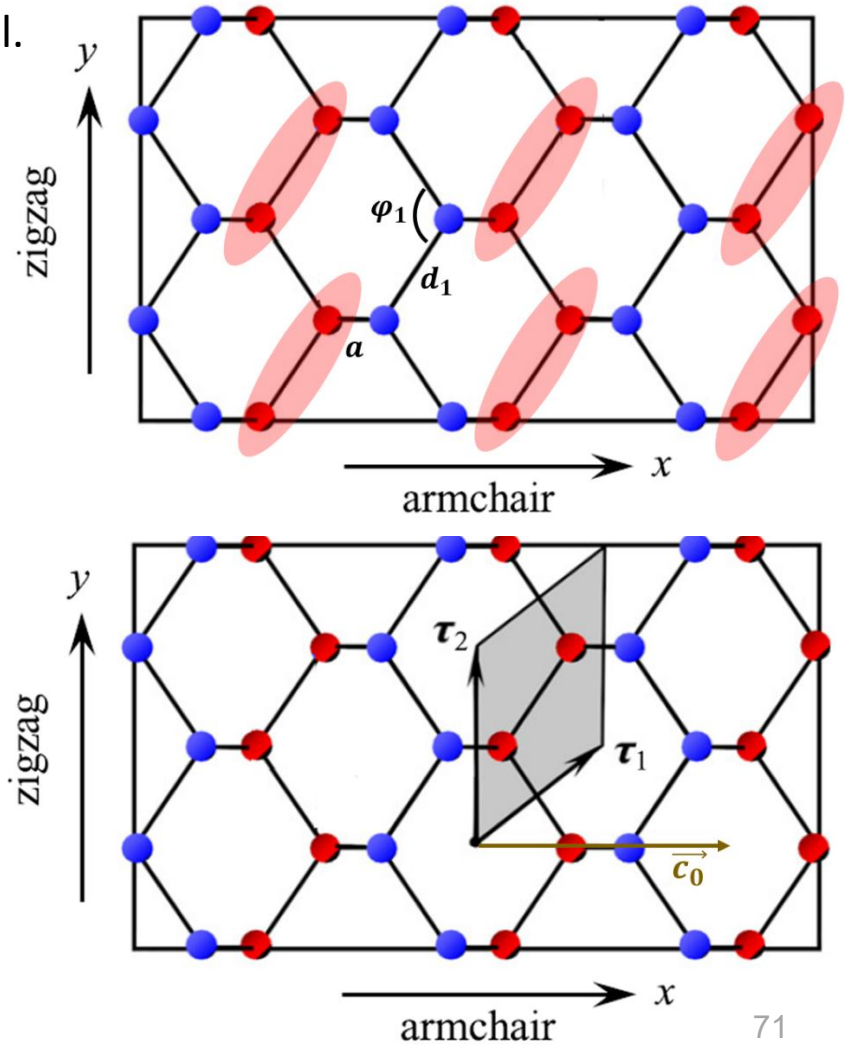

If we decompose the two vectors $\vec{\tau}_1$ and $\vec{\tau}_2$ along the x and y axes, and express their components in terms of a_0 and c_0, it is straightforward to verify that:

$$\overrightarrow{\tau_1} = \frac{c_0}{2}\widehat{u_x} + \frac{a_0}{2}\widehat{u_y}$$

$$\overrightarrow{\tau_2} = a_0\widehat{u_y}$$

5.5 PHOSPHORENE AND BLACK PHOSPHORUS

5.5.2 Primitive cell and Brillouin zone

If we repeat the same construction for the pairs of blue atoms, we obtain an equivalent result. The sum of the two parallelograms defines a new parallelogram that can be considered a **primitive cell** containing four phosphorus atoms.

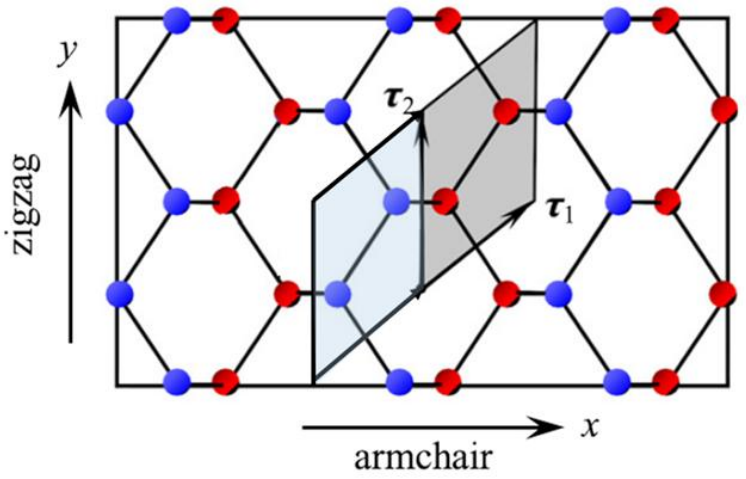

Its surface area is:

$$A = 2(\overrightarrow{\tau_1} \times \overrightarrow{\tau_2}) = 2\frac{a_0 c_0}{2} = a_0 c_0$$

$$\overrightarrow{\tau_1} = \frac{c_0}{2}\widehat{u_x} + \frac{a_0}{2}\widehat{u_y}$$

$$\overrightarrow{\tau_2} = a_0\widehat{u_y}$$

Thus, the two possible choices of primitive cell are equivalent in both area and number of atoms.

Let us now return to the original three-dimensional structure by placing the blue atoms back in the upper layer.

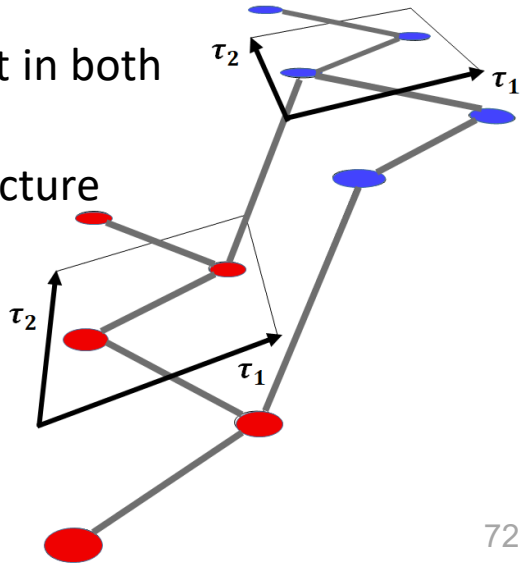

The full geometry of phosphorene is restored, and the two previously identified parallelograms are no longer coplanar but lie on two distinct layers, corresponding to the upper and lower sublayers of the crystal.

5.5 PHOSPHORENE AND BLACK PHOSPHORUS

5.5.2 Primitive cell and Brillouin zone

At this point, it is natural to recognize that the primitive cell can be described in terms of an orthorhombic structure:

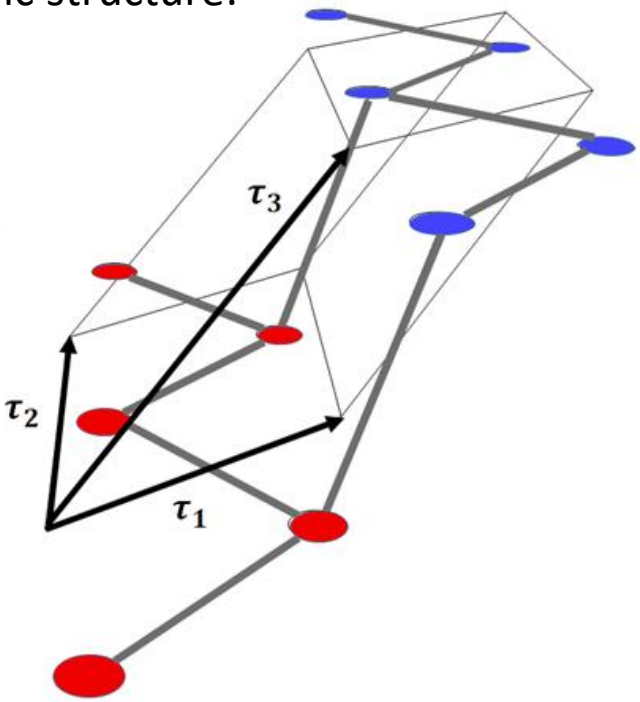

If we also construct the parallelepiped generated by the rectangle chosen as the fundamental cell:

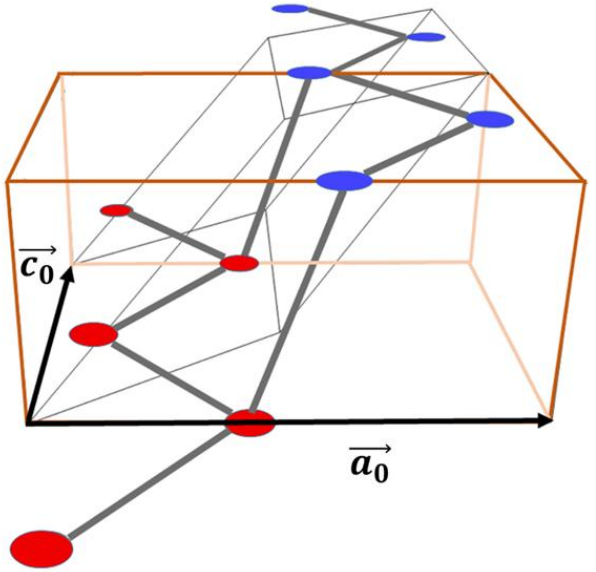

It is immediately evident that the orthorhombic structure occupies a smaller volume than the parallelepiped, making it a suitable candidate for the primitive cell containing four atoms.

5.5 PHOSPHORENE AND BLACK PHOSPHORUS

5.5.2 Primitive cell and Brillouin zone

The first Brillouin zone has two hexagonal faces in the $(k_z k_y)$ −plane.

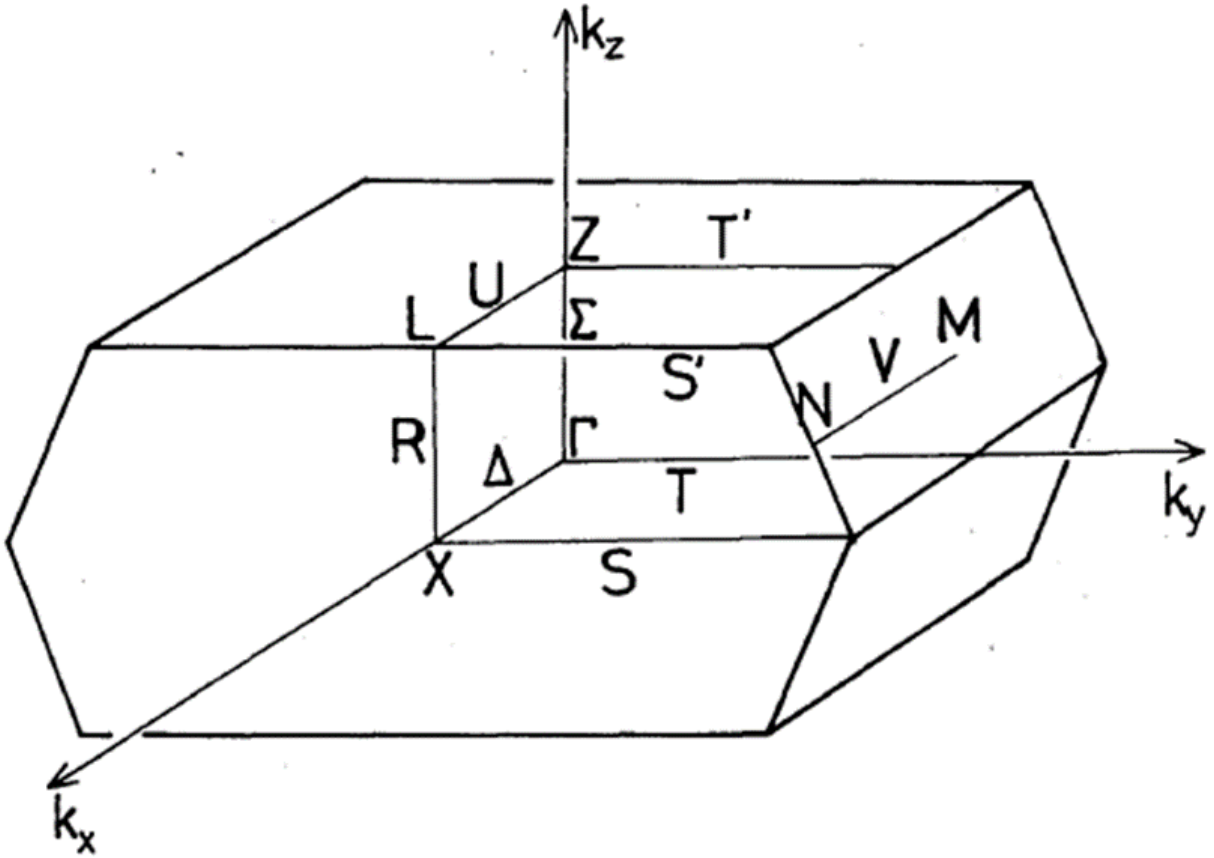

5.5 PHOSPHORENE AND BLACK PHOSPHORUS

5.5.3 Band Structure and Density of States

The method used to calculate the band structure of phosphorene is based on the **pseudopotential** approach.

Pseudopotential theory allows us to write the **Schrödinger equation** for the plane-wave component $\phi_{\vec{k}}^{v}(\vec{r})$ of the valence electron wavefunction:

$$(H + V^R)\phi_{\vec{k}}^{v}(\vec{r}) = \mathcal{E}_{\vec{k}}^{v}\phi_{\vec{k}}^{v}(\vec{r}) \qquad \text{with } H + V^R = -\frac{\hbar^2}{2m}\nabla^2 + V^{pseudo}$$

V^{pseudo} represents the effective periodic potential that replaces the true ionic potential U.

The assumption is that the pseudopotential is weak enough to justify treating the valence electrons within the nearly free electron approximation.

The simplest models assume a Coulomb potential at large distances and a constant potential in the core region. The matching point between the two regions is taken at the core radius r_c.

This form of the pseudopotential is overly simplistic and does not allow for an accurate reproduction of experimental data.

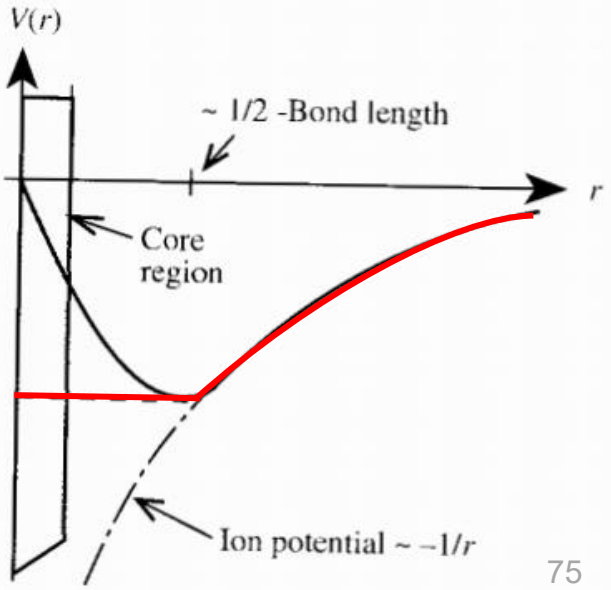

5.5 PHOSPHORENE AND BLACK PHOSPHORUS

5.5.3 Band Structure and Density of States

In 1973, Appelbaum and Hamann proposed a more accurate expression for the pseudopotential of a single Si^{4+} ion.

For the single ion, the **Appelbaum-Hamann pseudopotential** has the form:

$$V_{ion}(\vec{r}) = (V_1 + r^2 V_2)e^{-\alpha r^2}$$

where the parameters V_1, V_2 and α are determined by fitting to experimental data.

For phosphorus ions, these parameters take the values reported in the Figure.

If we use this expression for the pseudopotential to calculate the energy levels of a single phosphorus ion, we obtain excellent agreement with the experimentally measured energy levels.

	$3s$	$3p$	$3d$
Calculated	$(1s)$ -4.777	$(2p)$ -3.972	$(3d)$ -2.762
Experiment[13]	-4.778	-3.970	-2.920

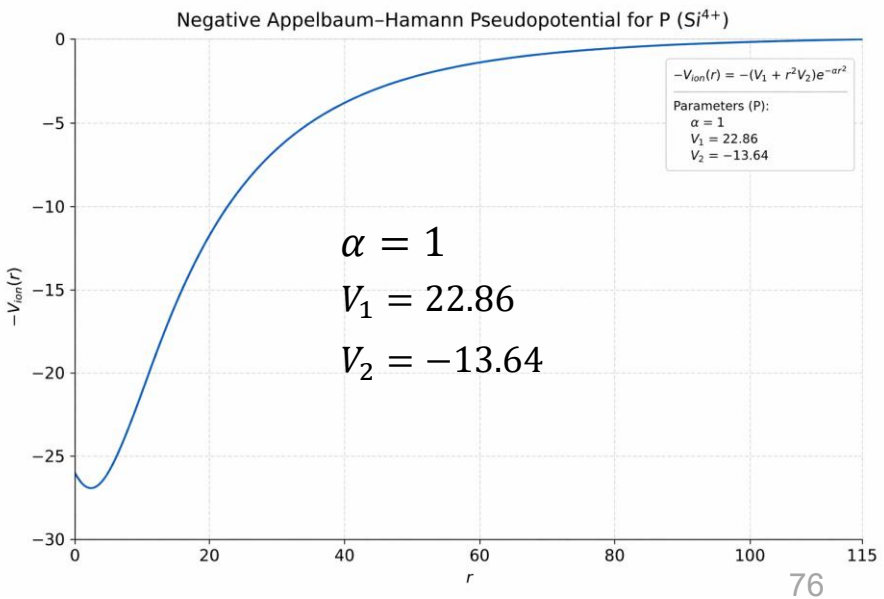

5.5 PHOSPHORENE AND BLACK PHOSPHORUS

5.5.3 Band Structure and Density of States

The pseudopotential approach has been highly successful in describing the energy bands and optical properties of a wide range of solids.

However, more accurate models must also account for the **nature of the bonding** (ionic, covalent, or mixed), since this directly affects the charge distribution.

A natural extension beyond the pseudopotential approach is therefore to include interaction terms that explicitly account for the electron charge distribution.

Calculating the **charge density** allows one to evaluate covalent bond charges and, consequently, to assess the degree of ionicity or the extent to which covalent bonds are modified by electrostatic interactions.

The calculation of charge density in semiconductor crystals was first addressed in 1971.

The **spatial distribution of the charge density** for the valence band n can be written as:

$$\rho_n(\vec{r}) = e \sum_{\vec{k}} \left| \phi^{v}_{n,\vec{k}}(\vec{r}) \right|^2$$

where the sum runs over all available states $\vec{k}$ in the band n.

The functions $\phi^{v}_{n,\vec{k}}$ are obtained from calculations based on pseudopotential method.

5.5 PHOSPHORENE AND BLACK PHOSPHORUS

5.5.3 Band Structure and Density of States

With these considerations, the **band structure** for phosphorene is obtained by solving the single-electron Schrödinger equation within the pseudopotential method:

$$\left[-\frac{\hbar^2}{2m}\nabla^2 + \sum_j V_{ion}\left(\vec{r} - \overrightarrow{R_j}\right) + V_H(\vec{r})\right]\phi^v_{n,\vec{k}}(\vec{r}) = \mathcal{E}_{n,\vec{k}}\phi^v_{n,\vec{k}}(\vec{r})$$

where $V_{ion}\left(\vec{r} - \overrightarrow{R_j}\right)$ is the Appelbaum-Hamann potential of the j-th ion located at $\overrightarrow{R_j}$.

The term $V_H(\vec{r})$ is the **Hartree potential**, determined by the valence charge density $\rho_n(\vec{r})$, obtained by solving the **Poisson equation**:

$$\nabla^2 V_H(\vec{r}) = -8\pi\rho_n(\vec{r}) \quad \text{with} \quad \rho_n(\vec{r}) = \sum_{\vec{k}} \left|\phi^v_{n,\vec{k}}(\vec{r})\right|^2$$

Within the pseudopotential method, the valence electron wave functions satisfy Bloch's theorem and can be expanded as:

$$\phi^v_{\vec{k}}(\vec{r}) = \frac{1}{\sqrt{\Omega}}\sum_{\vec{G}} c_{\vec{G}}\, e^{i(\vec{k}+\vec{G})\cdot\vec{r}}$$

where $\vec{G}$ are the reciprocal lattice vectors.

5.5 PHOSPHORENE AND BLACK PHOSPHORUS

5.5.3 Band Structure and Density of States

$$\left[-\frac{\hbar^2}{2m}\nabla^2+\sum_j V_{ion}\left(\vec{r}-\overrightarrow{R_j}\right)+V_H(\vec{r})\right]\phi^v_{n,\vec{k}}(\vec{r})=\varepsilon_{n,\vec{k}}\phi^v_{n,\vec{k}}(\vec{r})$$

$$\phi^v_{\vec{k}}(\vec{r})=\frac{1}{\sqrt{\Omega}}\sum_{\vec{G}} c_{\vec{G}}\, e^{i(\vec{k}+\vec{G})\cdot\vec{r}}$$

Substituting this form into the Schrödinger equation transforms the problem from real space into Fourier space. As a result, for each $\vec{k}$, one obtains a system of equations

$$\left[\varepsilon-\varepsilon^0_{\vec{k}-\overrightarrow{G_i}}\right]c_{\vec{k}-\overrightarrow{G_i}}=\sum_j U_{\overrightarrow{G_j}-\overrightarrow{G_i}}c_{\vec{k}-\overrightarrow{G_j}}$$

which can be solved to determine the **band structure of phosphorene**.

Since the primitive cell contains 4 phosphorus atoms and each atom contributes 5 valence electrons, **the lowest 10 bands are occupied**.

The **shaded region separates the valence band from the conduction band**.

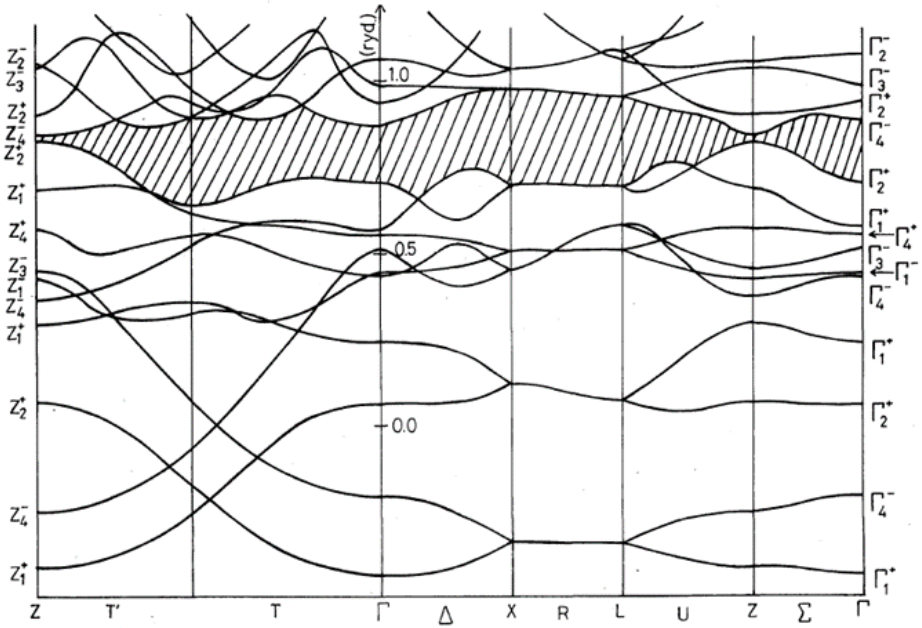

Fig. 4. The energy bands of black phosphorus.

5.5 PHOSPHORENE AND BLACK PHOSPHORUS

5.5.3 Band Structure and Density of States

Phosphorene is a **direct band-gap** semiconductor, with the minimum located at the Z point of the Brillouin zone (along the (001) direction).

At this point, the band gap is approximately 0.3 eV, and the dispersion can be locally approximated by a parabolic relation.

Along other directions, the band gap increases, reaching values up to about 3 eV; for example, at the Γ point it is around 2 eV.

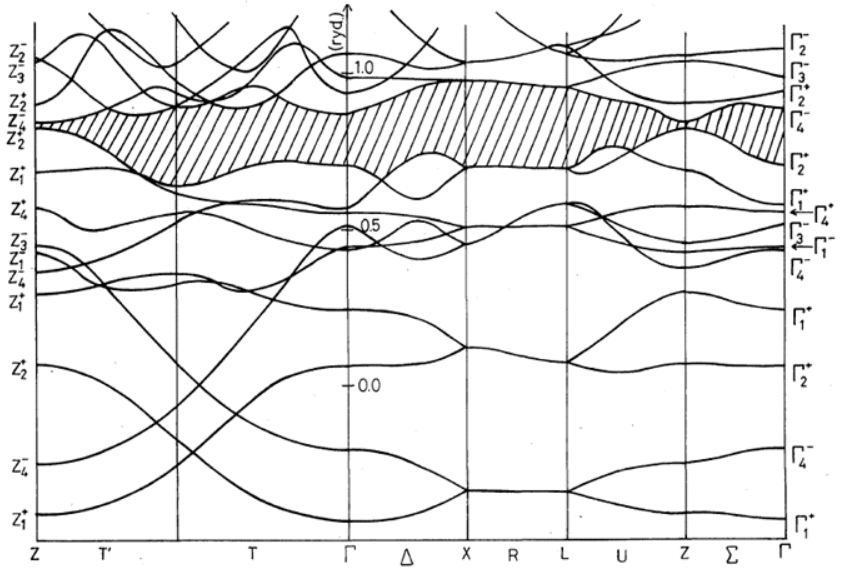

Fig. 4. The energy bands of black phosphorus.

Given the dispersion relations $\mathcal{E}_{n,\vec{k}}$, the density of states can be calculated:

The **density of states** of phosphorene exhibits a highly structured profile with multiple peaks, reflecting the anisotropic band dispersion and the presence of van Hove singularities.

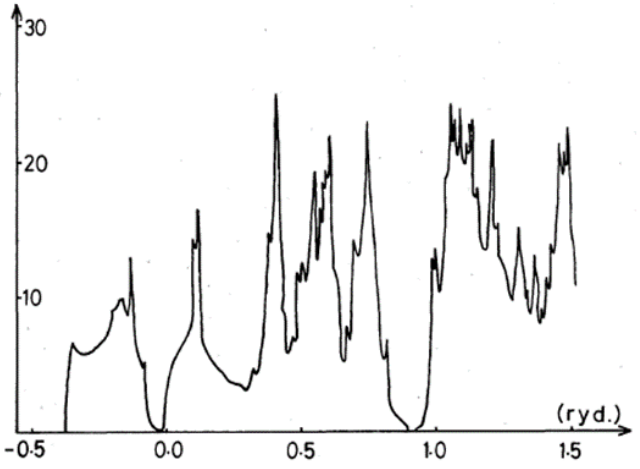

5.5 PHOSPHORENE AND BLACK PHOSPHORUS

5.5.3 Band Structure and Density of States

The **valence charge density** can be determined, represented in Figure as a contour map.

A **contour map** represents the charge density through lines connecting points of equal value. Closely spaced lines indicate rapid variations and high-density regions, while wider spacing corresponds to lower and more uniform charge distribution.

In phosphorene, the contour lines reflects the puckered structure and the **directional nature of the covalent bonds** between phosphorus atoms.

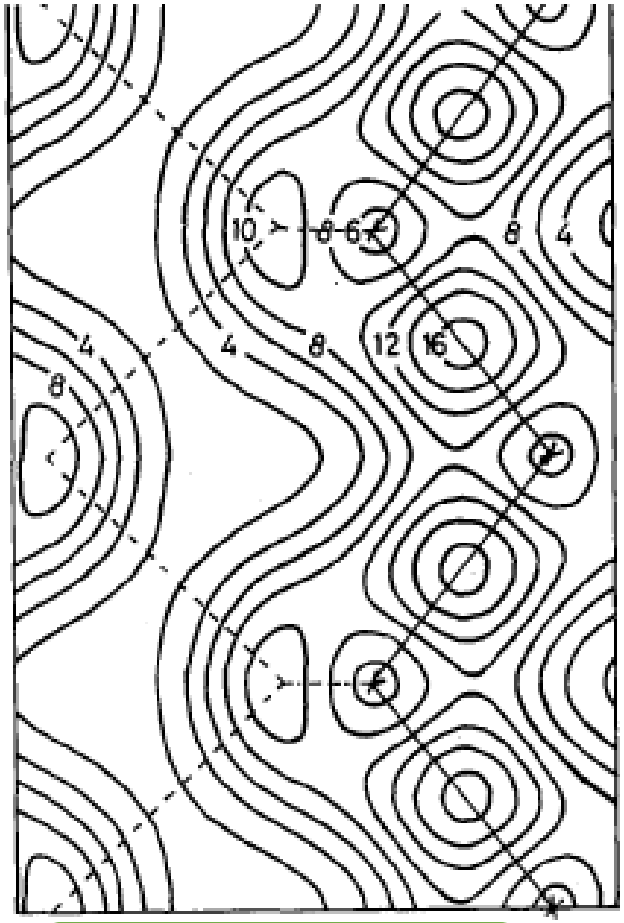

Also the effective mass of the electron and hole at the point Z can be estimated:

Table III. Calculated effective masses (m is the free electron mass).

	$\left(\frac{m^*}{m}\right)_x$	$\left(\frac{m^*}{m}\right)_y$	$\left(\frac{m^*}{m}\right)_z$	averaged
Hole	0.09	0.81	0.36	0.20
Electron	0.09	1.16	0.17	0.16

$$\rho_n(\vec{r}) = e \sum_{\vec{k}} \left|\phi^v_{n,\vec{k}}(\vec{r})\right|^2$$

5.5 PHOSPHORENE AND BLACK PHOSPHORUS

5.5.3 Band Structure and Density of States

If multiple layers of phosphorene are stacked to form **black phosphorus**, the resulting crystal exhibits a band gap that depends on the number of layers.
This effect was demonstrated through band structure calculations using the **GW method**.
The GW method is a many-body approach used to compute energy levels, expressed in terms of the single-particle Green's function G and the screened Coulomb interaction W.

Band structure for phosphorene using the GW approximation is shown in the right Figure.
Comparison of the calculation of the dispersion relations in the direction $\Gamma - \mathrm{X}$, using the pseudopotential method and the GW approximation is shown in the left Figure.

The GW method predicts a band gap of 1.6 eV, compared to 2.0 eV with pseudopotential.

At the Fermi level the relations are not so dissimilar.

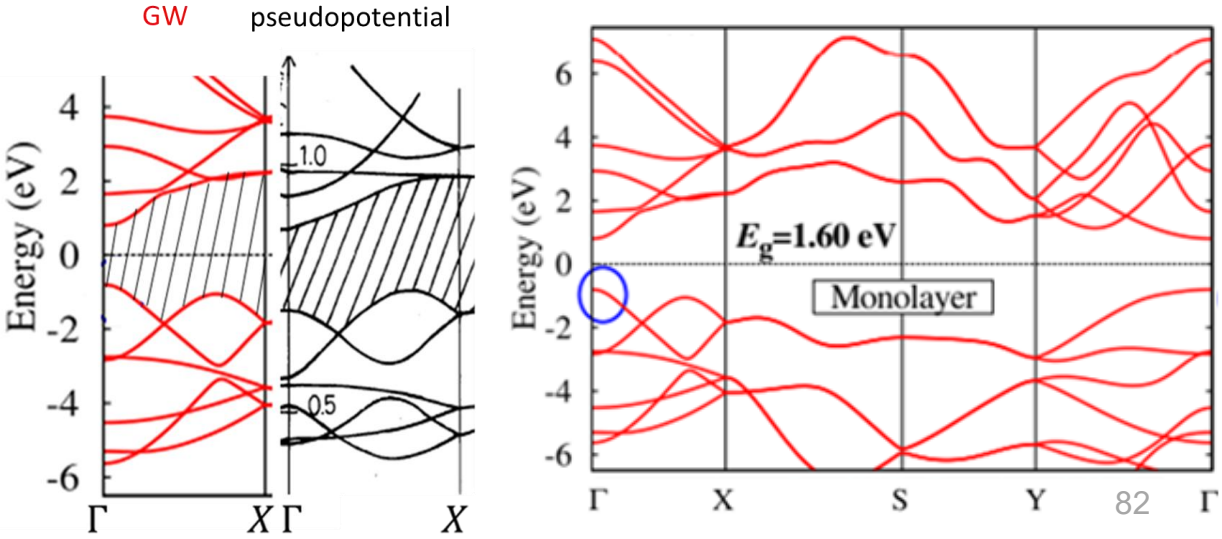

5.5 PHOSPHORENE AND BLACK PHOSPHORUS

5.5.3 Band Structure and Density of States

For multiple stacked layers of phosphorene, the energy gap at the Γ point decreases as the number of layers increases.

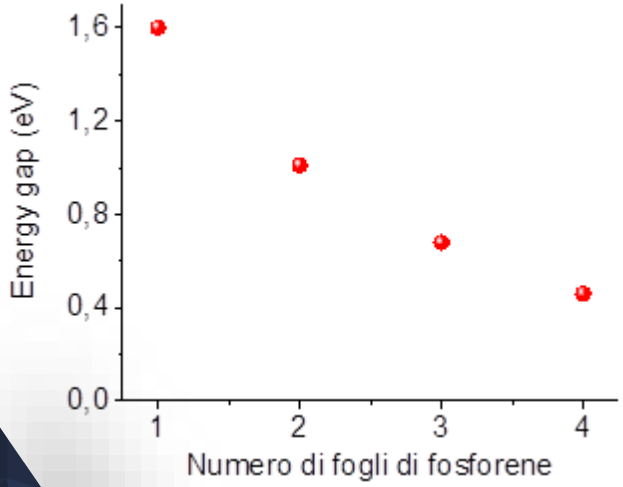

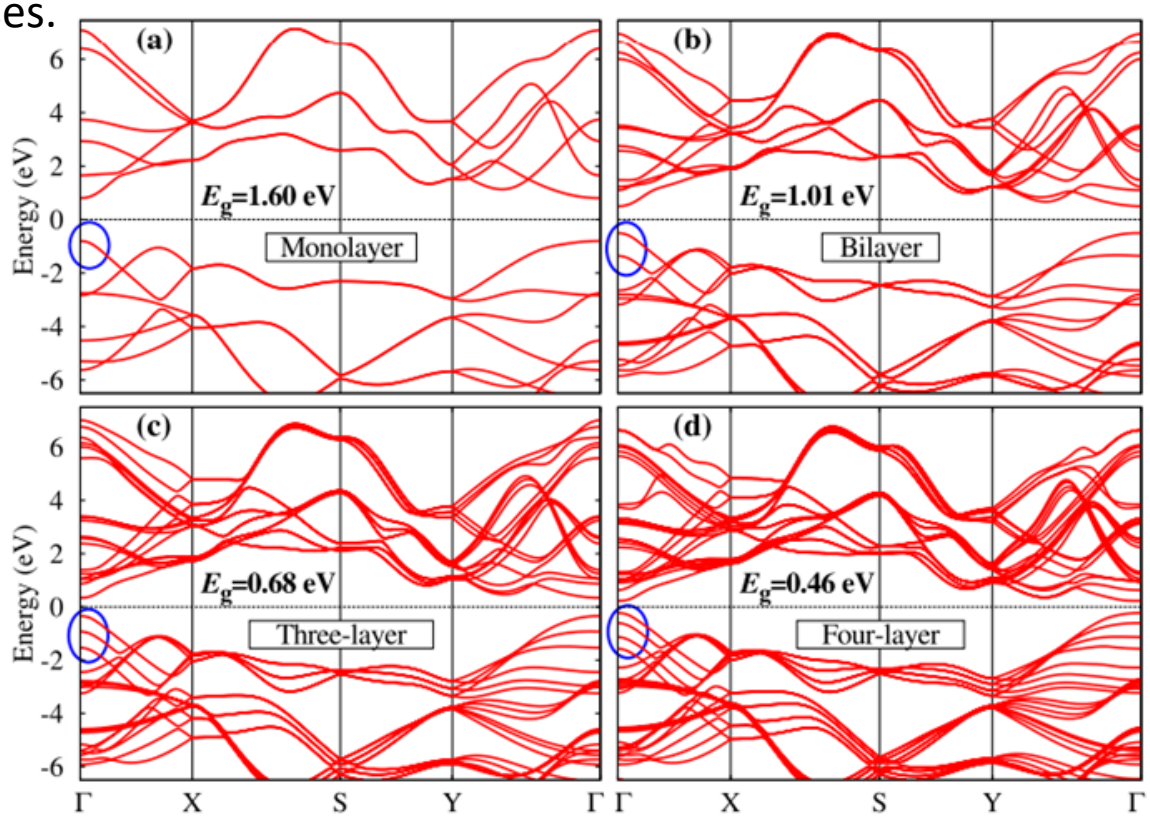

Black phosphorus, however, retains **a direct band gap regardless of the number of layers**.

5.5 PHOSPHORENE AND BLACK PHOSPHORUS

5.5.4 Field Effect Transistors

Black phosphorus can be used as an active material in **field-effect transistors**.

Transistors are the fundamental building blocks of modern electronic devices and integrated circuits. The discovery of graphene has sparked significant interest in the development of transistors based on two-dimensional materials.

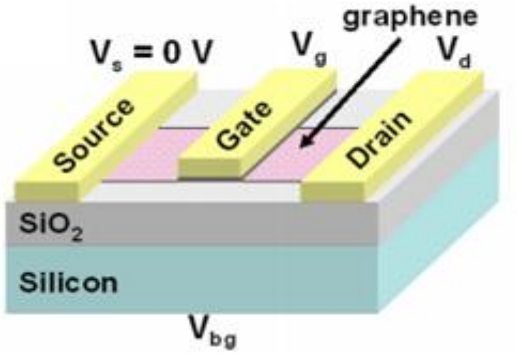

Graphene exhibits extremely high carrier mobility (up to $\sim 2 \times 10^4\ \mathrm{cm^2V^{-1}s^{-1}}$ at room temperature). However, due to the absence of an energy gap, it is not suitable for conventional logic applications.

Black phosphorus combines high carrier mobility with a large I_{ON}/I_{OFF} ratio.

In 2014, Zhang and Ye demonstrated the first FET based on black phosphorus with varying thicknesses, achieving a mobility of about $1000\ \mathrm{cm^2V^{-1}s^{-1}}$ for a 10 nm sample, higher than that of silicon.

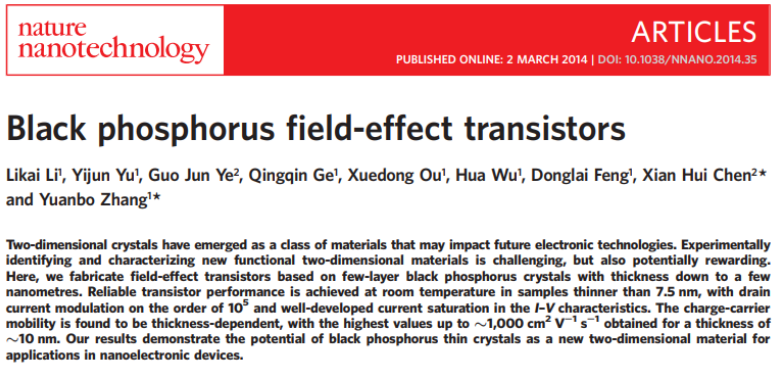
nature nanotechnology

ARTICLES

PUBLISHED ONLINE: 2 MARCH 2014 | DOI: 10.1038/NNANO.2014.35

Black phosphorus field-effect transistors

Likai Li[1], Yijun Yu[1], Guo Jun Ye[2], Qingqin Ge[1], Xuedong Ou[1], Hua Wu[1], Donglai Feng[1], Xian Hui Chen[2]* and Yuanbo Zhang[1]*

Two-dimensional crystals have emerged as a class of materials that may impact future electronic technologies. Experimentally identifying and characterizing new functional two-dimensional materials is challenging, but also potentially rewarding. Here, we fabricate field-effect transistors based on few-layer black phosphorus crystals with thickness down to a few nanometres. Reliable transistor performance is achieved at room temperature in samples thinner than 7.5 nm, with drain current modulation on the order of 10^5 and well-developed current saturation in the *I–V* characteristics. The charge-carrier mobility is found to be thickness-dependent, with the highest values up to ~1,000 $cm^2\ V^{-1}\ s^{-1}$ obtained for a thickness of ~10 nm. Our results demonstrate the potential of black phosphorus thin crystals as a new two-dimensional material for applications in nanoelectronic devices.

5.5 PHOSPHORENE AND BLACK PHOSPHORUS

5.5.4 Field Effect Transistors

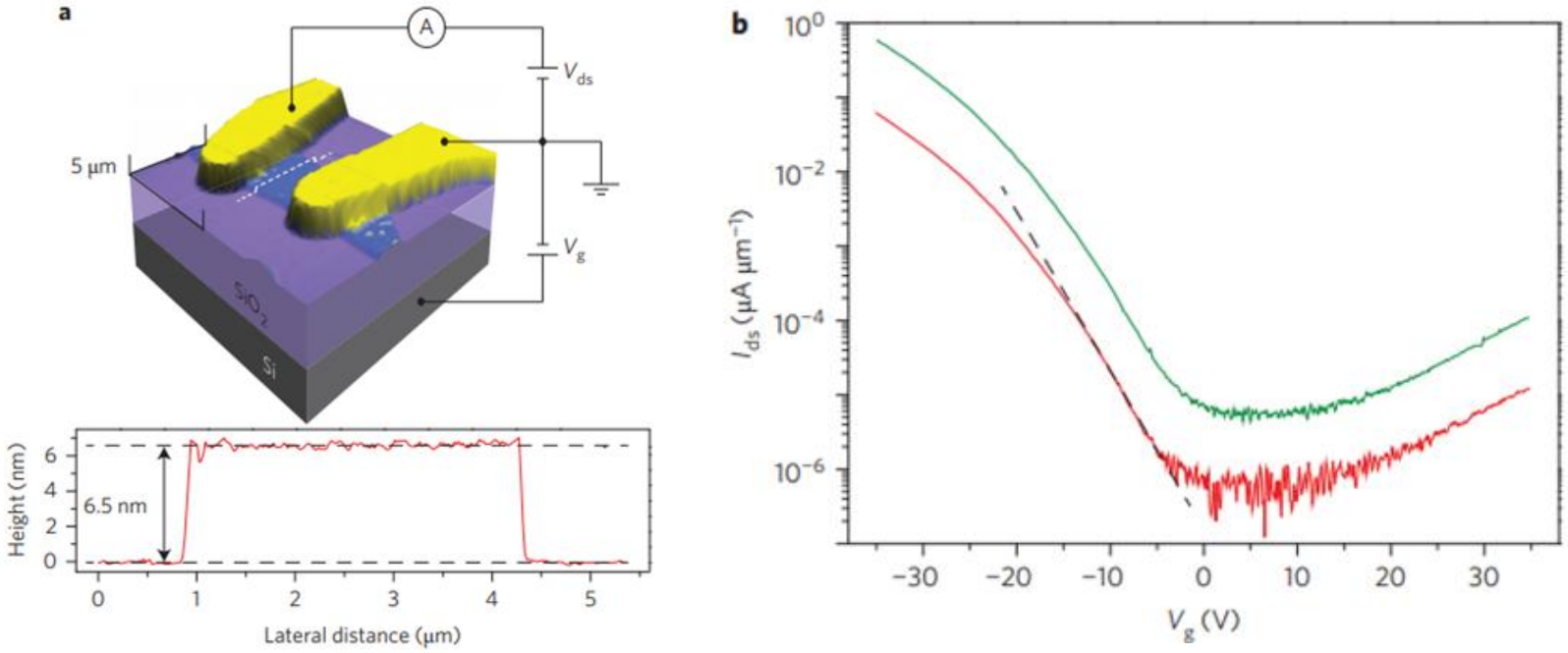

Compared to graphene, black phosphorus exhibits lower carrier mobility; however, its I_{ON}/I_{OFF} ratio is nearly four orders of magnitude higher.

As shown in Fig. b, when the gate voltage is varied from −30 V to 0 V, the channel switches from the “on” state to the “off” state, with the drain current decreasing by about **five orders of magnitude**.

5.5 PHOSPHORENE AND BLACK PHOSPHORUS

5.5.5 Photodetectors

Due to its thickness-dependent direct band gap—ranging from about 0.35to 2.0 eV (from multilayer to monolayer phosphorene)—**black phosphorus is an excellent candidate for photodetectors** operating over a broad spectral range, from the visible to the infrared.

The black-phosphorus photodetector is based on a back-gate FET configuration.

Materials Views
www.MaterialsViews.com

ADVANCED MATERIALS
www.advmat.de

Broadband Black-Phosphorus Photodetectors with High Responsivity

*Mingqiang Huang, Mingliang Wang, Cheng Chen, Zongwei Ma, Xuefei Li, Junbo Han, and Yanqing Wu**

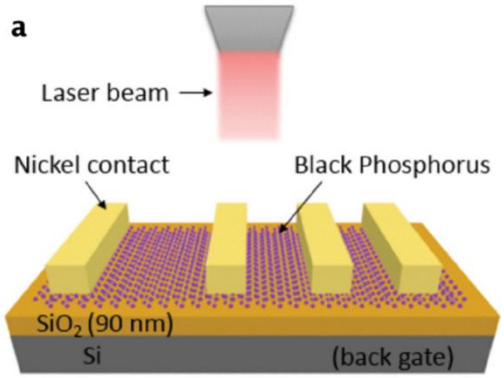

The responsivity strongly depends on temperature.